International Journal of Computational and Experimental Science and ENgineering (IJCESEN)

Vol. 11-No.4 (2025) pp. 7350-7378
http://dergipark.org.tr/en/pub/ijcesen

ISSN: 2149-9144

Research Article

Copyright © IJCESEN

Seismic Retrofitting of Non-Compliant RC Structures Using SMA Bracings and Modified DDBD: A Parametric Approach

Marwa Bakhouche[1]*, Rafik Madi [2], Moufida Gherdaoui[3] , Abderrahim Labed[4]

[1] Civil Engineering and Hydraulic Laboratory, University of 8 Mai 1945, P.B. 401, Guelma, 24000, Algeria
*** Corresponding Author Email:** bakhouche.marwa@univ-guelma.dz - **ORCID:** 0000-0001-9372-9789
[2] Civil Engineering and Hydraulic Laboratory, University of 8 Mai 1945, P.B. 401, Guelma, 24000, Algeria
Email: madi.rafik@univ-guelma.dz - **ORCID:** 0000-0001-7849-8599

[3] Department of Civil Engineering, University Abbes Laghrour P. O. Box 1252, Khenchela, Algeria
Email: ghardaoui.moufida@univ-khenchela.dz - **ORCID:** 0000-0003-0088-4283

[4] Civil Engineering Department, University of Tebessa, Tebessa, Algeria
Email: abderrahim@univ-tebessa.dz- **ORCID:** 0000-0001-7313-7065

Article Info:

DOI: 10.22399/ijcesen.4011
Received: 28 May 2025
Accepted: 10 September 2025

Keywords

Seismic retrofitting,
Shape Memory Alloy bracings,
Direct Displacement-Based Design,
Nonlinear static pushover analysis,
Nonlinear time history analysis,
reinforced concrete structures

Abstract:

This paper introduces a novel seismic retrofitting strategy using Shape Memory Alloy (SMA) bracings within a modified Direct Displacement-Based Design (DDBD) framework for non-compliant reinforced concrete (RC) structures. SMA bracings, characterised by superelasticity and energy dissipation, were investigated through parametric analyses considering various configurations, cross-sectional areas, and damping properties. Nonlinear static pushover and nonlinear time history analyses were performed on mid-rise (six-storey) and high-rise (nine-storey) RC buildings. Results indicated that optimal X-bracing designs—1250 mm² cross-sectional area with 0.10 damping for six-storey, and 1600 mm² with 0.15 damping for nine-storey structures—markedly enhanced seismic resilience. Improvements included increased global ductility, reduced inter-storey drifts, and better control of plastic hinge formation. Retrofitted six-storey structures achieved reductions of 94% in peak floor accelerations (PFA) and 95% in residual displacements, while nine-storey structures showed 94% and 63% reductions, respectively. Comparisons with conventional steel bracings confirmed SMA's superior performance. SMA bracings reduced residual displacements by 70% (six-storey) and 63% (nine-storey), compared to 50% with steel. They also improved global ductility by 35% and 40%, whereas steel achieved only moderate gains. These outcomes highlight SMA bracing's effectiveness in controlling deformations, enabling recentering, and minimizing permanent damage. Although the study was applied to real Algerian structures, findings can be generalized to RC buildings of varying heights worldwide. SMA bracings emerge as a scalable and cost-efficient solution for seismic-prone regions. Future work should address applications to steel and hybrid structures and assess SMA's long-term performance under different seismic conditions.

1. Introduction

Seismic retrofitting of existing reinforced concrete (RC) structures that do not comply with modern seismic design codes remains a

critical challenge in many seismic-prone regions globally, including Algeria. Many buildings in Algeria constructed before implementing the RPA99/2003 seismic code (Algériennes, 2003) were designed to support gravity loads only and consequently needed more features to resist medium to high-magnitude earthquakes. As a result, these buildings present significant safety risks, making seismic retrofitting crucial to minimize damage, prevent structural failure, and protect lives during future seismic events.

Over the decades, various retrofitting techniques have been proposed and explored, with self-centering systems emerging as one of the most promising methods for improving seismic resilience (Qian et al., 2016); (Wang & Zhu, 2018); (Kari et al., 2011). These systems have the unique ability to recenter structures after seismic events, significantly reducing residual deformations and ensuring better serviceability. Among these methods, Shape Memory Alloy (SMA) bracings have garnered particular attention due to their exceptional superelasticity, enabling them to undergo large deformations and return to their original shape upon unloading. SMA bracings also possess excellent energy dissipation properties, which make them highly effective in seismic retrofitting applications.

Extensive research has confirmed the potential of SMA bracings in improving seismic performance. (Miller et al., 2012) demonstrated the stable hysteretic response of SMA bracings under cyclic loading, highlighting their higher energy dissipation capacity. Similarly, (Moradi et al., 2014) found that SMA bracings provided superior recentering behaviour compared to buckling-restrained braces (BRBs), reducing residual drifts. (Asgarian & Moradi, 2011) further demonstrated that incorporating short SMA segments in steel bracings can reduce inter-storey drift ratios (IDRs) and residual inter-storey drift ratios (RIDRs), further confirming the effectiveness of SMA technology in retrofitting applications.

Recent studies have expanded on these findings by exploring innovative SMA technologies. For instance, (Ferraioli et al., 2022); (Ferraioli & Lavino, 2018) evaluated the seismic performance of an RC building retrofitted with SMA dampers. They confirmed their ability to limit transient and residual inter-storey drifts, significantly improving seismic resilience. (Miani, 2021) highlighted the application of SMA bracings in historical buildings, showing that SMA technologies reduce force demand and preserve sensitive structures' architectural integrity.

Moreover, (Abraik & Asif, 2023) investigated utilization design ratios (UDRs) for SMA bracings in concentrically braced frames (CBFs). They found that optimizing UDR configurations minimizes material use while maintaining SMA bracings' unique recentering and energy dissipation characteristics. Similarly, Vignoli et al. analysed SMA composites to improve energy dissipation in earthquake-resistant structures, highlighting their superior performance to traditional materials. Lastly, (Matari et al., 2023) applied SMA bracings to retrofit historical RC structures, demonstrating significant reductions in displacements, stresses, and accelerations during seismic events.

Despite these advancements, integrating SMA bracings within the Direct Displacement-Based Design (DDBD) framework still needs to be explored, particularly for retrofitting non-compliant RC structures in regions with high seismic activity, such as Algeria. The DDBD method, pioneered by (Calvi et al., 2008), emphasizes controlling building displacements during seismic events by setting target displacements as performance objectives. While several studies have applied DDBD with traditional steel bracing systems (e.g., (Bergami & Nuti, 2013); (Mazza & Vulcano, 2014); (Mazza, 2014)), the integration of SMA bracings, with their unique superelastic behaviour and flag-shaped hysteresis loops, has not been fully explored within this framework. Recent work by (Monti et al., 2024) offers a promising approach for the seismic retrofit of RC buildings using dissipative bracings, specifically targeting gravity-load-designed (GLD) RC frames—similar to the older structures in Algeria. Their non-iterative design method effectively reduces inter-storey drifts, protecting existing columns from seismic damage. Using a simplified "stick model" for modal analysis, they optimize bracing systems regarding stiffness and damping. This efficient methodology is relevant to the present study, as it offers a practical approach to improving seismic performance in structures facing similar challenges. Similarly, (Alehojjat et al., 2023) investigate residual inter-storey drift ratio (RIDR) demands in mid-rise steel structures equipped with fluid viscous dampers (FVDs)

using the DDBD approach. Their focus on residual drifts aligns to minimize permanent deformations after seismic events, a key concern in retrofitting structures in high-seismicity regions. Through nonlinear time-history analyses, they propose a modified equation for estimating RIDR demands, which could be adapted for use in this study's integration of SMA bracings within a DDBD framework.

This study addresses this research gap by integrating SMA bracings into a modified DDBD framework. A comprehensive parametric analysis evaluates the effects of different SMA bracing configurations, cross-sectional areas, and damping properties on the seismic performance of mid-rise (six-storey) and high-rise (nine-storey) non-compliant RC structures. Focusing on key performance indicators such as global ductility, inter-storey drift, and peak floor acceleration, this study aims to demonstrate how SMA bracings can significantly improve seismic resilience and ensure compliance with the RPA99/2003 seismic code. The findings of this research have broader implications for retrofitting strategies in other seismic-prone regions worldwide.

2. Modified DDBD Procedure for RC Structures with SMA Bracings

For this study, we based our design on the DDBD method by [14], adapting it to integrate SMA bracings for retrofitting non-compliant RC structures in Algeria. This modification leverages the unique properties of SMA, such as elasticity and shape retention, to improve seismic resistance.

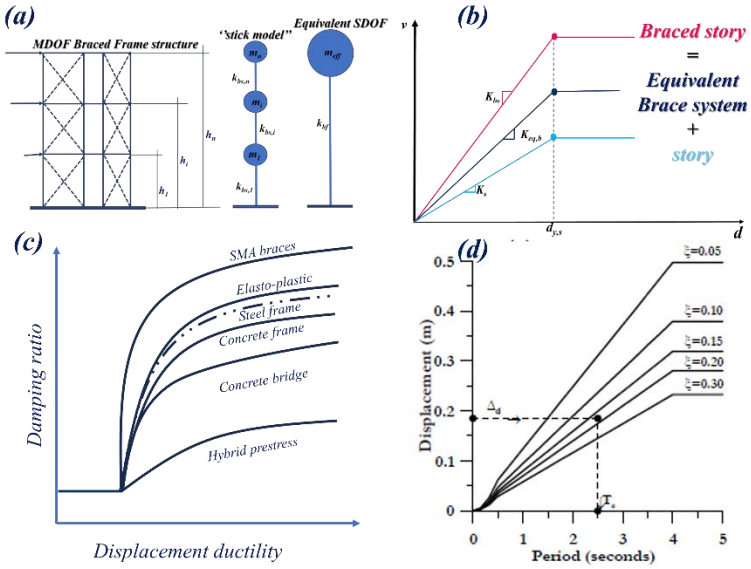


Figure. 1: *Incorporation of SMA Bracings in the DDBD Method.*

The suggested process in this paper follows the standard DDBD approach, modelling the MDOF structure as an SDOF system (**Figure 1a**). The SDOF system is enhanced by incorporating an SMA bracing, which modifies the structure's stiffness and damping characteristics (**Figure 1b**), improving rigidity and vibration absorption. A key aspect is establishing a relationship between the equivalent viscous damping and the desired ductility level, reflecting the impact of the SMA bracings (**Figure 1c**). The effective time period (Te) at peak displacement is calculated using the design displacement spectra, modified to account for SMA bracings' enhanced damping (**Figure 1d**). This adjustment further improves seismic performance. The following are the steps in the modified DDBD for RC Structures with SMA Bracings:

Step 1: Determination of Design Displacement (Δ_d)

The design displacement of the structure is determined by the maximum displacement or drift of the most essential part of the structure and its assumed form of displacement. The design displacement Δ_d is expressed as a function of m_i and Δ_i, according to the following equation:

$$\Delta_d = \sum_{i=1}^{n} \frac{m_i \Delta_i^2}{m_i \Delta_i} \quad (1)$$

where Δ_i is the displacement at each storey derived from the inelastic mode shape (δ_i) As provided in Eqs. (3 and 4), proportionate to critical storey displacement (Δ_c) and mode shape in the crucial storey level (δ_c), designed using inter-storey drift limit (θ_d) It is mainly derived from code specifications (RPA99/2003).

$$\Delta_i = \delta_i \left(\frac{\Delta c}{\delta_c}\right) \quad (2)$$

$$\text{For } n \leq 4;\ \delta_i = \frac{H_i}{H_n} \quad (3)$$

$$\text{For } n > 4;\ \delta_i = \frac{4}{3}\left(\frac{H_i}{H_n}\right)\left(1 - \frac{H_i}{4H_n}\right) \quad (4)$$

H_n represents the overall height of the building, H_i represents the height of the most significant storey, and m_i represents the mass at every considerable level i.

Step 2: Introduction of Drift Reduction Factor (γ)

A drift reduction factor γ accounts for higher mode effects to ensure the target displacement reflects structural behaviour accurately. It is based on the building's total height (H_n) And modifies the design displacement in each storey: $\Delta_{i,w} = \gamma \Delta_i$ (5)

$$\gamma = 1.15 - 0.0034 H_n \quad (6)$$

Step 3: Calculation of Effective Mass (m_{eff}) and Effective Height (H_{eff})

- **Effective Mass m_{eff}:**

The effective mass is determined by the mass of each floor and the bracings, distributed evenly along the structure:

$$m_{eff} = \frac{\sum_{i=1}^{n} m_i . h_i + m_{SMA\ braces} . h_{SMA\ braces}}{H_t} \quad (7)$$

- **Effective Height H_{eff}:**

Similarly, effective height is calculated considering floor and bracing heights:

$$h_{eff} = \frac{\sum_{i=1}^{n} h_i . k_i + h_{SMA\ braces} \cdot k_{SMA\ braces}}{k_t} \quad (8)$$

Where: k_i : lateral stiffness of the i-th floor

$k_{SMA\ bracings}$: lateral stiffness of the bracings

k_t : total lateral stiffness of the structure

Step 4: Design Ductility (μ)

Design ductility (μ) measures the structure's ability to undergo deformation without losing integrity. It is based on the design displacement. Δ_d, yield displacement Δ_y, Behavior of SMA bracings.

To account for SMA bracings, the yield displacement is adjusted as follows:

$$\Delta_{y,Adj} = \Delta_y + \Delta_{SMAB} \quad (9)$$

Where: Δ_{SMA} is the contribution from SMA bracings, calculated using the Superelastic properties of SMA materials. This involves calculating the stress difference. $\Delta_\sigma = \sigma_{MS} - \sigma_{AS}$, strain difference $\Delta_\varepsilon = \epsilon_{MS} - \varepsilon_{AS}$, and Superelastic plateau strain length

$$\epsilon_L : \Delta_{SMAB} = \frac{\Delta_\sigma}{EA} . \frac{\Delta_\varepsilon}{EM} . \epsilon_L \quad (10)$$

Where: EA: Young's Modulus (Austenite), EM: Young's Modulus (Martensite)

Finally, design ductility is calculated as:

$$\mu = \frac{\Delta_d}{\Delta_{y,Adj}} \quad (11)$$

Step 5: Equivalent Viscous Damping (ξ_{eq})

Equivalent viscous damping ξ_{eq} is critical in seismic design, representing the structure's energy dissipation capacity. To determine ξ_{eq} for the DDBD method with SMA bracings:

Effective Stiffness (k_{eff}) : Effective stiffness (k_{eff}) is the sum of the structure's stiffness k_s and the stiffness contribution from SMA bracings k_{SMAB} :

$$k_{eff} = k_s + k_{SMAB} \quad (12)$$

$$k_{SMAB} = \frac{EA_{SMA}}{L_{SMAB}} \quad (13)$$

Where:

L_{SMAB} : The length of the SMA bracings.

Equivalent Damping Coefficient (C_{eq}): includes damping from SMA bracings and other sources:

$$C_{eq} = C_{SMA} + C_{other} \quad (14)$$

C_{SMA} is determined using the SMA material's energy dissipation coefficient (η):

$$C_{SMA} = \eta . \frac{2\sqrt{m_e k_e}}{1 + (\omega_n \xi_{SMA})^2} \quad (15)$$

Where: η The energy dissipation coefficient of the SMA material = $\frac{\varepsilon_r}{\varepsilon_L}$, ω_n the natural frequency of the structure, and ξ_{SMA} The damping ratio of the SMA bracings = $\frac{\sigma_{Af} - \sigma_{As}}{\sigma_{Mf} - \sigma_{Ms}}$

Finally, equivalent viscous damping is:

$$\xi_{eq} = \frac{C_{eq}}{2\sqrt{m_e k_e}} \quad (16)$$

Step 6: Calculation of Effective Period (T_e)

The effective period at peak displacement is determined using design displacement spectra, modified for the contribution of SMA bracings, as shown in **Figure.1d**. Standard spectra are based on 5% damping (Eurocode 8 [20]; UBC 97 [21]). To adjust for a different damping level ξ_{eq} the following equation is used:

$$\Delta_{(T,\xi_{eq})} = \Delta_{(T,5)} * \left(\frac{10}{5+\xi_{eq}}\right)^{0.5} \quad (17)$$

Where: $\Delta_{(T,\xi_{eq})}$: Displacement at calculated ξ_{eq}, $\Delta_{(T,5)}$: 5% design spectra, ξ_{eq}: Equivalent Viscous Damping, T: Period

a) Step 7: Calculation of Base Shear Force (V_b)

Base shear force (V_b) represents the total lateral force due to seismic activity and is calculated as:

$$V_b = k_{eff}.\Delta_d \quad (18)$$

b) Step 8: Distribution of Base Shear Force (V_b)

Base shear force V_b is distributed across the structure's height to ensure that each level can withstand seismic loads, promoting earthquake-resistant construction.

Determination of Distribution Factors: Calculate modal mass participation factors ($\emptyset_i$) For each vibration mode, consider SMA bracings. The distribution factor (DF_i) for each mode, "i" is determined as:

$$DF_i = \frac{\emptyset_i}{\sum_{i=1}^{n}\emptyset_i} \times \frac{\psi_i}{\sum_{i=1}^{n}\psi_i} \quad (19)$$

Distribute V_b

The base shear force at each level (V_{bi}) is calculated by multiplying the total base shear force (V_b) with the distribution factors for each mode "i":

$$V_{bi} = DF_i \times V_b \quad (20)$$

After distributing the base shear forces, the building is analysed to determine the flexural strength needed at potential plastic hinge locations. Plastic hinges form in predetermined areas by applying capacity-based design principles in the modified DDBD method, ensuring controlled deformation during seismic events. This approach achieves two key goals: compliance with the RPA99/2003 Algerian seismic code and a performance level that prioritizes life safety by limiting structural damage. The method not only meets regulations but also enhances the resilience of non-compliant RC structures against seismic forces.

3. Case study: application of the proposed design methodology to non-compliant RC structures

3.1 Description of the buildings

The case study examines two RC structures in Zone III under the Algerian seismic code RPA99/2003. Initially designed for gravity loads, the buildings have a rectangular layout with five bays of 5 meters each. The structures consist of six stories (six stories) and nine stories (nine stories), with a uniform storey height of 3.06 meters (**Figures. 2a, 2b, and 2c** show the elevations and plans). The structural system includes 150 mm thick concrete slabs supported by beams and columns. **Table 1** provides details of the beams and columns, with materials having a steel strength of 300 MPa and concrete strength of 25 MPa.

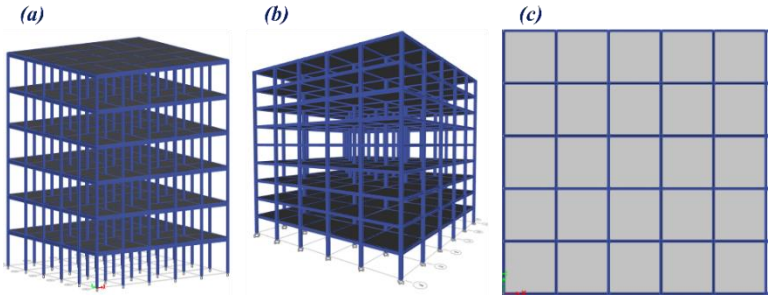


Figure. 2 *Framing Elevation and plan of the studied buildings.*

Table 1. *Details of structural members for both buildings.*

Structure	Member	Storey	Cross section (cm^2)	Longitudinal reinforcement	Transverse reinforcement

				Top	Bottom	
Six-storey	Beam	Ground -2	20 x 45	3-12Φ	3-12 Φ	8 Φ@100 c/c
		3-5	25 x 45	4-12Φ	4-12 Φ	8 Φ@150 c/c
Nine-storey	Beam	Ground -3	20 x 45	3-14Φ	3-14 Φ	8 Φ@100 c/c
		4-7	25 x 45	4-14Φ	4-14 Φ	8 Φ@150 c/c
Six-storey	column	Ground	25 x 25	12-16 Φ		8 Φ@100 c/c
		1-2	20 x 20	12-14 Φ		8 Φ@100 c/c
		3-5	20 x 20	12-12 Φ		8 Φ@150 c/c
Nine-storey	column	Ground	30 x 30	12-20 Φ		8 Φ@100 c/c
		1-3	35 x 35	12-16 Φ		8 Φ@100 c/c
		4-7	30 x 30	12-14 Φ		8 Φ@150 c/c

3.2 Numerical modelling

A 3D numerical model of the buildings for the case study was developed using the finite element software package ETABS [22]. Five (05) distinct scenarios of the buildings are examined in this study:

Table 2. *The different scenarios being considered in the study.*

Scenario	*Description*
1. Non-retrofitted of Non-compliant Structure	A non-retrofitted and non-compliant reinforced concrete (RC) structure representing an existing building that does not meet current seismic design codes and standards in Algeria. This serves as a baseline for assessing seismic performance deficiencies.
2. Evaluation of Bracing Configurations	Investigation of three different bracing configurations for seismic retrofitting using SMA bracings: X-bracing (concentric), V-bracing (chevron), and diagonal bracing.
3. Variation of Cross-sectional Area of SMA Bracings	Evaluation of three different cross-sectional areas of the SMA bracings: 750 mm² (low stiffness), 1250 mm² (medium stiffness), and 1600 mm² (high stiffness).
4. Variation of Damping Properties of SMA Bracings	Investigation of three different damping levels of the SMA bracings: low damping (0.05, narrower hysteresis loop, lower energy dissipation), medium damping (0.10), and high damping (0.15, wider hysteresis loop, higher energy dissipation).
5. Optimal Seismic Retrofitting Solution	A combination of the best-performing configurations, cross-sectional areas, and damping properties identified from the previous scenarios will be used to develop an optimal seismic retrofitting solution using SMA bracings for the non-compliant RC structure.

For each parametric case (scenarios 1-4), pushover analyses will be conducted on both structures to determine the optimal scenario for cross-sectional area, damping, and bracing configuration, ensuring compliance with RPA99/2003 and meeting life safety criteria. In scenario 5, the best-performing SMA bracing properties will be used to retrofit the non-compliant structure, followed by a Nonlinear Time History Analysis (NLTHA) to compare the performance of both the non-retrofitted (scenario 1) and retrofitted (scenario 5) structures.

The simulation of beams and columns uses the Mander unconfined concrete model for compressive stress-strain behaviour and the Park model for reinforcing steel. Nonlinear behaviour is modelled with displacement-controlled lumped plastic hinges, considering axial force, bi-axial bending (P-M-M), and moment-rotation (M-θ) relationships. Points A-E represent force-displacement behaviour (**Figure. 3**). The DDBD method quantifies performance based on damage, with performance levels (IO, LS, CP) defined by FEMA-356 [23]. Plastic hinge lengths are set as 0.5 times the section depth, as suggested by Pauley and Priestley [24]. **Table 3** presents comprehensive information on the acceptable requirements for performance levels, damage stages, and their corresponding drift constraints.

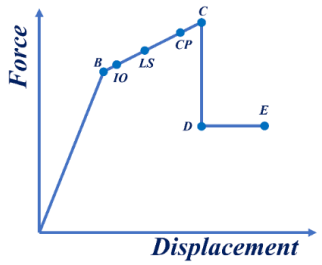


Figure.3 *Force-Deformation and Acceptable Criteria [23]*

Table 3. *Acceptable Criteria for Performance Levels [23]*

Performance levels	Damage state	Drift limitations
Immediate occupancy (IO)	No damage	1%
Life safety (LS)	Repair damage	2-2.5%
Collapse prevention (CP)	Severe damage	>2.5%

3.3 Details of the retrofit method

SMA bracings are innovative devices used for seismic retrofitting. They leverage super elasticity and energy dissipation to enhance earthquake resistance. They exhibit a flag-shaped hysteresis, making them ideal for seismic applications.

3.3.1 Mechanical properties of SMA bracings

SMA bracings, typically made from nickel-titanium (NiTi) alloys, possess super elasticity, shape memory effect, and excellent energy dissipation. Their mechanical properties are determined by composition and thermomechanical treatment. In this study, the mechanical properties used for SMA bracings are derived from the Experimental Investigation of Mechanical Properties of NiTi Superelastic SMA Cables by Lian et al. [25]. **Table 4** outlines critical properties, including transformation temperatures (As, Af, Ms, Mf) and stress thresholds (σAs, σAf, σMs, σMf).

Figure. 4a shows the phase transformation behaviour, while **Figure. 4b** illustrates the stress-strain response, highlighting SMAs' super elasticity, which allows them to recover shape after significant strain.

Table 4 *summarizes the critical mechanical properties of the NiTi-based SMA material used in this study.*

Property	Value
Austenitic Start Temperature (A_s)	-10 °C
Austenitic Finish Temperature (A_f)	18 °C
Martensitic Start Temperature (M_s)	14 °C
Martensitic Finish Temperature (M_f)	-16 °C
Austenitic Start Stress (σ_{As})	195 MPa
Austenitic Finish Stress (σ_{Af})	165 MPa
Martensitic Start Stress (σ_{Ms})	420 MPa
Martensitic Finish Stress (σ_{Mf})	450 MPa
Austenitic Strain at Start (ε_{As})	0.013125
Austenitic Strain at Finish (ε_{Af})	0.09025
Martensitic Strain at Start (ε_{Ms})	0.078653
Martensitic Strain at Finish (ε_{Mf})	0.005156
Superelastic Plateau Strain Length (ε_L)	0.07
Maximum Residual Strain (ε_r)	6%
Young's Modulus (Austenite) (E_A)	32000 MPa
Young's Modulus (Martensite) (E_M)	22222 MPa

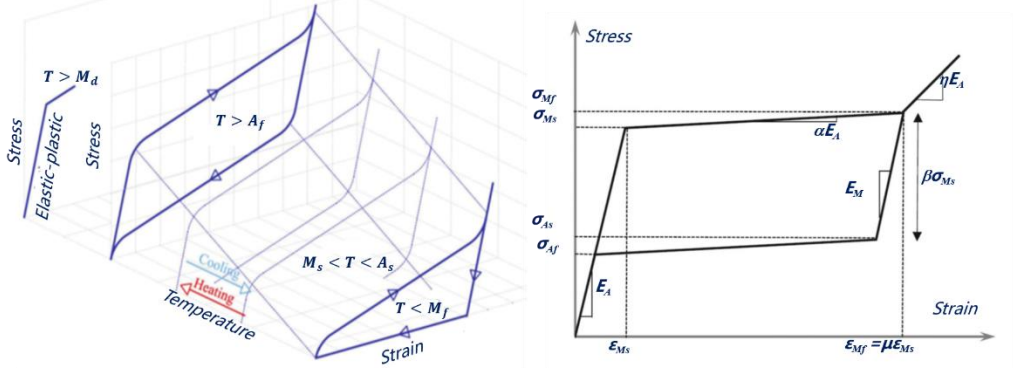


Figure. 4 ***a)*** *Superelastic Behaviour and* ***b)*** *Phase Transformation of SMA.*

3.3.2 Modelling and identification of material

SMA bracing hysteresis behaviour was accurately modelled using multi-linear plastic and elastic link properties in ETABS. The plastic link (**Figure. 5a**) models the hysteresis loop, capturing energy dissipation, while the elastic link (**Figure. 5b**) models the flag-shaped force-deformation response. Parameters like unloading stiffness and residual strain (εr) were calibrated to represent the SMA bracing behaviour in seismic conditions accurately.

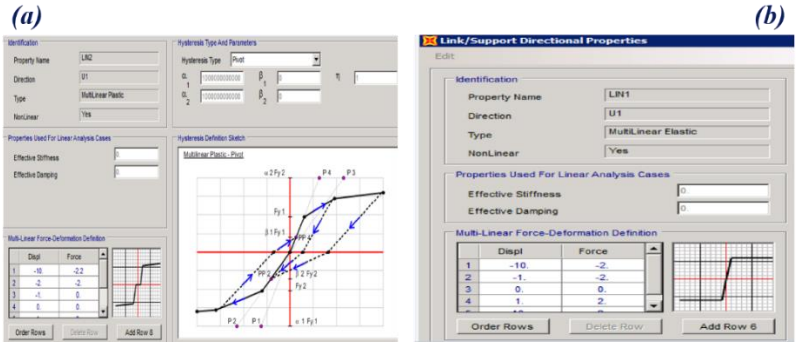


Figure. 5 ***a)*** *Multi-linear Plastic link property using Pivot hysteresis,* ***b)*** *Multi-linear Elastic link property [26].*

3.4 Seismic ground motions

Seven ground motions were selected from the Pacific Earthquake Engineering Research (PEER) NGA database [27] based on the location of the studied structure. **Table 5** provides the specifics of these accelerograms. The motions were matched to meet the response spectrum from RPA99/2003 [1] for a rock site (S2) in Seismic Zone III, with a peak ground acceleration (PGA) of 0.4g. Spectra-compatible time histories were generated using the academic version of SeismoMatch software [28], as shown in **Figure 6. Table 5** includes details of the selected ground motions, such as name, year, record length, time steps, station, and magnitude.

Table 5 *Characteristics of Earthquakes used in NLTHA*

Serial N°	Earthquake name	Year	Records	Time step (s)	Station name	Magnitude
1	Morgan Hill	4/24/1984	RSN453	0.005	Fremont - Mission San Jose	5.01
2	Chalfant Valley	7/21/1986	RSN555	0.005	Mammoth Lakes Sheriff Subst	5.5
3	Landers	6/28/1992	RSN838	0.02	Barstow	6.53
4	Big Bear	6/28/1992	RSN910	0.02	Joshua Tree	6.6
5	Kobe Japan	1995	RSN1114	0.01	Port Island	6.9
6	Chi-Chi Taiwan	1999	RSN 1200	0.02	CHY033	7.2
7	Boumardes	5/21/2003	RSN 12345	0.02	Dar el Beida	6.8

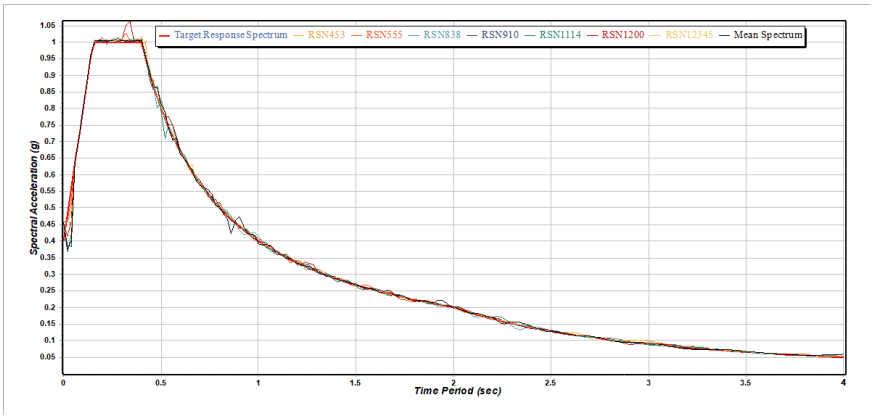


Figure.6 *Matched ground motions with target response spectrum [28].*

4. Results and discussions

This study uses NLSA for scenarios 1-4 to evaluate different SMA bracing configurations,

cross-sectional areas, and damping properties to find the best retrofitting solution. Scenario 5 involves NLTHA using the best configurations from previous scenarios. NLTHA compares seismic performance between un-retrofitted (scenario 1) and optimally retrofitted (scenario 5) structures under seven selected ground motions. Results focus on capacity curves, performance point, and plastic hinge distribution, inter-storey drifts, global ductility, peak floor acceleration, residual displacement, and displacement profiles. This demonstrates the modified DDBD framework's effectiveness in improving seismic resilience for non-compliant RC structures in Algeria.

4.1 Non-linear static "pushover" analysis Results

The NLSA assesses the seismic performance of retrofitted and non-retrofitted RC structures with SMA bracings. Capacity curves and performance points are analysed to evaluate deformation capacity, inter-storey drift ratios, and failure mechanisms. These results are crucial to identifying optimal SMA bracing configurations and assessing their effectiveness in seismic retrofitting. The following sections present the detailed findings, highlighting improvements achieved through SMA bracings.

a. Capacity curves

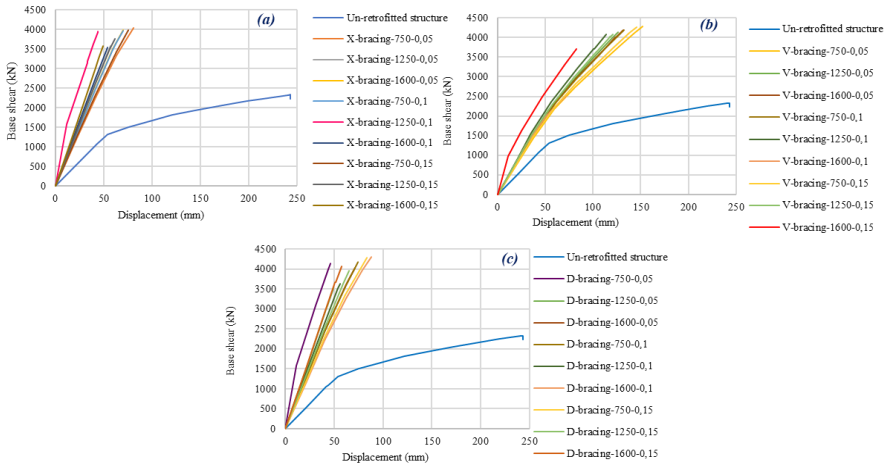


Figure. 7 *Capacity curve for a six-storey structure, a) X-bracing, b) V-bracing, and c) diagonal bracing.*

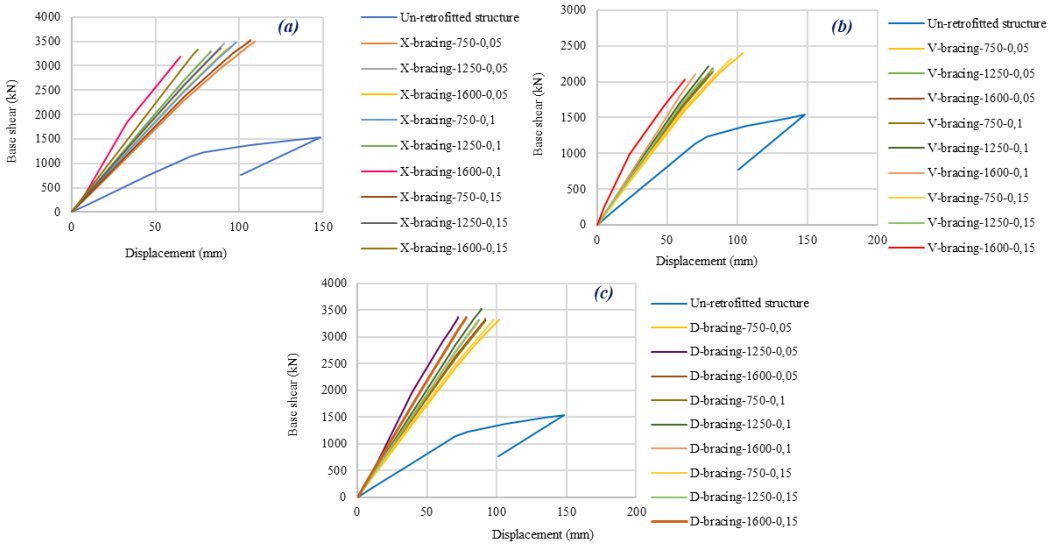


Figure. 8 *Capacity curve for nine-storey structure, a) X-bracing, b) V-bracing, and c) diagonal bracing.*

The pushover curves in **Figures. 7** and **8** demonstrate the effectiveness of incorporating SMA bracing in the DDBD framework to enhance seismic performance in non-compliant RC structures in Algeria. For the six-storey structure (**Figure. 7**), X-bracing (1250 mm², 0.1 damping) improves base shear capacity by 200%, balancing stiffness, strength, and energy dissipation. V-br

acing with a 1600 mm² cross-section and 0.15 d amping increases base shear by 140%, while di agonal bracing with a 750 mm² cross-section an d 0.05 damping provides flexibility and minimi zes weight.

For the nine-storey structure, X-bracing with a 1600 mm² cross-section and 0.10 damping deli vers the necessary stiffness and energy dissipat ion. V-bracing with the same cross-section and 0.15 damping offers strength and ductility for g reater seismic demands. In contrast, diagonal br acing with a 1250 mm² cross-section and 0.05 d amping manages lateral forces with controlled f lexibility.

b. Performance Point and Plastic Hinge Distribution

The performance point and plastic hinge distribution analyses provide vital insights into the effectiveness of the different bracing configurations in enhancing the seismic performance of RC structures.

The un-retrofitted structure shows high displacement (215.016 mm) and base shear capacity (2230.27 kN), with numerous plastic hinges in the CP region, highlighting the need for retrofitting. For the six-storey structure, X-bracing (**Table 6**), especially the 1250 mm^2 cross-section and 0.1 damping, improves performance, with most hinges in the IO range and none in the CP range. V-bracing (**Table 7**) also performs well, especially the (1250 mm², 0.1 damping) and (1600 mm^2, 0.1 damping) configurations, with minimal CP-level hinges and efficient energy dissipation. Lower-capacity configurations like V-bracing (750 mm^2, 0.05 damping) show more CP-level hinges, making them less effective. Diagonal bracing results (**Table 8**) are mixed: D-bracing (750 mm^2, 0.05 damping) and D-bracing (1250 mm^2, 0.05 damping) perform well at the IO and LS levels, but higher-capacity configurations like D-bracing (1600 mm^2, 0.1 damping) show more CP-level hinges, indicating vulnerabilities.

Table 6. *Performance Point and Plastic Hinge Distribution for Retrofitted and Un-Retrofitted Six-storey Structure with X-Bracing SMA Systems.*

Case	Performance point displacement (mm)	Performance point base shear (kN)	Hinges in IO	Hinges in LS	Hinges in CP	Hinges beyond CP	Remarks	Number of Hinges Formed	Location of First Hinge	Final Hinge Distribution
Un-retrofitted structure	215,016	2230,2738	124	300	500	228	Significant non-compliance problems	1152	Ground floor column	Poor distribution, many in CP and beyond CP
X-bracing-750-0,05	77,813	3935,513	875	140	60	0	Improved performance	1075	Mid-height column	Majority IO, fewer LS, minimal CP
X-bracing-1250-0,05	62,878	3657,7196	800	200	50	0	Good performance	1050	Upper floor beam	Majority IO, some LS, minimal CP
X-bracing-1600-0,05	68,212	3915,6658	700	300	30	0	Similar to 1250-0.05	1030	Mid-height column	Majority IO, fewer LS, and no beyond CP
X-bracing-750-0,1	71,634	3685.083	820	160	20	0	Improved performance	1000	Ground floor column	Majority IO, fewer LS, and minimal CP

X-bracing-1250-0,1	39,336	3636,0573	600	200	0	0	Best performing case	800	Ground floor beams	Majority IO, some LS, no CP
X-bracing-1600-0,1	65,545	3786,6935	750	220	30	0	Slightly worse than 1250-0.05	1000	Ground floor beams	Majority IO, some LS, very few CP
X-bracing-750-0,15	74,684	3808,9127	720	260	20	0	Good performance	1000	Ground floor beams	Majority IO, some LS, very few CP
X-bracing-1250-0,15	56,315	3512,1093	770	220	10	0	Near to best performance	1000	Ground floor beams	Majority IO, few LS, and CP
X-bracing-1600-0,15	54,1	3889,2558	710	225	0	0	Good performance, not the best	935	Ground floor beams	Majority IO, some LS

Table 7 *Performance Point and Plastic Hinge Distribution for Retrofitted and Un-Retrofitted Six-storey Structure with V-Bracing SMA Systems.*

Case	Performance point displacement (mm)	Performance point base shear (kN)	Hinges in IO	Hinges in LS	Hinges in CP	Hinges beyond CP	Remarks	Number of Hinges Formed	Location of First Hinge	Final Hinge Distribution
Un-retrofitted structure	215,016	1533,8839	124	300	500	228	Significant non-compliance problems	1152	Ground floor column	Poor distribution, many in CP and beyond CP
V-bracing-750-0,05	124,738	3718,7156	500	350	150	20	Improved performance	1020	Mid-height column	Predominantly IO, fewer in CP
V-bracing-1250-0,05	97,462	3919,5715	550	300	100	10	Better performance	960	Mid-height column	More IO, fewer in CP and beyond CP
V-bracing-1600-0,05	108,143	3619,4708	600	280	80	0	Similar to 1250-0.05	960	Ground floor beams	Majority IO, fewer LS, and CP
V-bracing-750-0,1	121,563	3948,2197	700	250	50	0	Better due to higher bracing capacity	1000	Ground floor beams	Majority IO, fewer LS, and CP
V-bracing-1250-0,1	103,654	3829,651	600	200	0	0	Best performing case	800	Ground floor beams	Majority IO, some LS, no CP
V-bracing-1600-0,1	63,141	2358,5509	928	76	0	0	Near best performance case	1004	Ground floor beam	Majority IO, minimal LS, and no CP

V-bracing-750-0,15	116,787	3542,6651	550	450	52	0	Good performance	1052	Upper floor column	Majority IO, fewer LS, some CP
V-bracing-1250-0,15	100,13	3901,5874	500	500	47	0	Near best performance case	1047	Mid-height beams	Majority IO, fewer LS, some CP
V-bracing-1600-0,15	86,834	3573,8931	751	50	0	0	Best performing case	801	Mid-height beam	Majority IO, minimal LS, and no CP

Table 8 *Performance Point and Plastic Hinge Distribution for Retrofitted and Un-Retrofitted Six-storey Structure with Diagonal-Bracing SMA Systems.*

Case	Performance point displacement (mm)	Performance point base shear (kN)	Hinges in IO	Hinges in LS	Hinges in CP	Hinges beyond CP	Remarks	Number of Hinges Formed	Location of First Hinge	Final Hinge Distribution
Un-retrofitted structure	215,016	2230,2738	124	300	500	228	Significant non-compliance problems	1152	Ground floor column	Poor distribution, many in CP and beyond CP
D-bracing-750-0,05	43,941	4060,2603	502	442	0	0	Best performance, fewer hinges	944	Ground Floor Beams	Uniform distribution, mostly in beams
D-bracing-1250-0,05	61,850	3188,1969	520	440	85	5	Moderate performance, some hinges in CP	1050	Second Floor Beams	Concentrated in lower and mid-levels
D-bracing-1600-0,05	63,413	3675,4039	580	500	120	30	Many hinges, significant damage	1230	Ground Floor Columns	Spread across all stories
D-bracing-750-0,1	63,213	3318,7554	600	520	130	50	High hinge count, less desirable	1300	First Floor Columns	Significant spread, higher stories
D-bracing-1250-0,1	67,978	3431,7334	560	480	110	20	More hinges, higher damage potential	1170	Ground Floor Beams	Spread across all stories
D-bracing-1600-0,1	66,046	3800,8734	640	560	160	70	Worst performance, many hinges beyond CP	1430	Ground Floor Columns	Significant spread, higher stories
D-bracing-750-0,15	66,179	3441,1264	620	540	150	60	Many hinges beyond CP	1370	Ground Floor Beams	Significant spread, higher

D-bracing-1250-0,15	64,9144	3309,9651	540	460	100	10	Higher hinge count, less effective	1110	Ground Floor Columns	Spread across all stories
D-bracing-1600-0,15	56,535	3886,5796	505	435	50	0	Good performance, slightly more hinges	990	First Floor Beams	Concentrated on lower stories

For the nine-storey structure, X-bracing (**Table 9**) significantly enhances seismic performance, particularly with the (1250 mm^2, 0.1 damping) and (1600 mm^2, 0.15 damping) configurations, reducing displacements and placing most hinges in the IO and LS ranges. V-bracing **(Table 10)** also performs well, but lower-capacity configurations, such as V-bracing (750 mm^2, 0.05 damping), show more CP-level hinges. Diagonal bracing (**Table 11**) shows variable results, with some configurations like D-bracing (1600 mm^2, 0.15 damping) performing well, but others, like D-bracing (750 mm^2, 0.1 damping), exhibiting more CP-level hinges.

Table 9. *Performance Point and Plastic Hinge Distribution for Retrofitted and Un-Retrofitted Nine-storey Structure with X-Bracing SMA Systems.*

Case	Performance point displacement (mm)	Performance point base shear (kN)	Hinges in IO	Hinges in LS	Hinges in CP	Hinges beyond CP	Remarks	Number of Hinges Formed	Location of First Hinge	Final Hinge Distribution
Un-retrofitted structure	143,791	1521,8896	1696	26	54	46	Non-compliant, high number of hinges	1822	Ground Floor Columns	Majority in lower and mid-levels
X-bracing-750-0,05	104,583	3370,7042	890	780	190	28	Worst performance, many hinges beyond CP	1888	Ground Floor Columns	Significant spread, higher stories
X-bracing-1250-0,05	90,934	3444,0336	733	539	98	15	Best performance, fewer hinges beyond CP	1385	Second Floor Beams	Concentrated in lower and mid-levels
X-bracing-1600-0,05	93,277	3353,6298	809	537	64	18	More hinges, higher damage potential	1428	Ground Floor Beams	Spread across all stories
X-bracing-750-0,1	96,895	3276,6652	777	650	128	35	High hinge count, less desirable	1590	First Floor Columns	Significant spread, higher stories
X-bracing-1250-0,1	86,787	3311,9540	795	337	72	8	Best performance, fewer hinges in CP	1212	Ground Floor Beams	Spread across all stories

X-bracing-1600-0,1	63,83	3161,9279	792	210	0	0	Best performing case	1002	Ground Floor beams	Majority IO, some LS, no CP
X-bracing-750-0,15	100,334	3263,5975	820	680	140	12	Many hinges beyond CP	1652	Ground Floor Beams	Significant spread, higher stories
X-bracing-1250-0,15	89,962	3411,5944	722	498	82	6	Moderate performance, fewer hinges	1308	Ground Floor Beams	Uniform distribution, mostly in beams
X-bracing-1600-0,15	73,724	3099,5942	665	523	10	0	Better performance, moderate hinges	1198		

Table 10 *Performance Point and Plastic Hinge Distribution for Retrofitted and Un-Retrofitted nine-story Structure with V-Bracing SMA Systems.*

Case	Performance point displacement (mm)	Performance point base shear (kN)	Hinges in IO	Hinges in LS	Hinges in CP	Hinges beyond CP	Remarks	Number of Hinges Formed	Location of First Hinge	Final Hinge Distribution
Un-retrofitted structure	143,791	1521,8896	1696	26	54	46	Non-compliant, high number of hinges	1822	Ground Floor Columns	Majority in lower and mid-levels
V-bracing-750-0,05	99,369	4228,4333	837	628	48	39	Higher hinge count, less desirable	1552	First Floor Columns	Significant spread, higher stories
V-bracing-1250-0,05	80,03	4119,8703	701	590	41	20	Moderate number of hinges beyond CP	1352	Ground Floor Beams	Significant spread, higher stories
V-bracing-1600-0,05	80,042	4000,0703	710	597	154	36	A higher number of hinges count	1497	First Floor Columns	Significant spread, higher stories
V-bracing-750-0,1	96,367	4176,1123	615	672	90	25	Higher hinge count, less effective	1402	Ground Floor Beams	Spread across all stories
V-bracing-1250-0,1	78,052	4275,5671	520	587	30	15	Moderate number of hinges beyond CP	1152	Ground Floor Beams	Significant spread, higher stories
V-bracing-1600-0,1	65,425	3950,3004	627	383	10	0	Good performance, few hinges in CP	1020	Ground Floor Beams	Uniform distribution, mostly in beams
V-bracing-750-0,15	98,368	4210,993	619	740	102	29	More hinges, higher	1490	Ground Floor Columns	Spread across all stories

							damage potential			
V-bracing-1250-0,15	79,531	4138,1993	607	566	57	20	Better performance, moderate hinges	1250	second Floor Beams	Concentrated in lower and mid-levels
V-bracing-1600-0,15	57,823	38883,8343	530	462	0	0	Best performance, no hinges beyond CP	992	Ground Floor beams	Majority IO, some LS, no CP

Table 11 *Performance Point and Plastic Hinge Distribution for Retrofitted and Un-Retrofitted nine-storey Structure with Diagonal-Bracing SMA Systems.*

Case	Performance point displacement (mm)	Performance point base shear (kN)	Hinges in IO	Hinges in LS	Hinges in CP	Hinges beyond CP	Remarks	Number of Hinges Formed	Location of First Hinge	Final Hinge Distribution
Un-retrofitted structure	143,791	1521,8896	1696	26	54	46	Non-compliant, high number of hinges	1822	Ground Floor Columns	Majority in lower and mid-levels
D-bracing-750-0,05	No Performance Point	No Performance Point	800	370	298	100	No performance points, maximum damage	1568	First Floor Columns	Significant spread, higher stories
D-bracing-1250-0,05	69,121	3078,2373	600	697	0	0	Best performance, no hinges in CP or beyond CP	1297	Ground Floor Beams	Concentrated on lower stories
D-bracing-1600-0,05	88,708	3230,6593	640	580	120	65	Higher hinge count, less desirable	1405	First Floor Columns	Significant spread, higher stories
D-bracing-750-0,1	90,96	3033,4445	798	210	357	87	Better performance, moderate hinges	1452	Second Floor Beams	Concentrated in lower and mid-levels
D-bracing-1250-0,1	99,495	3263,0449	704	572	81	44	Moderate performance hinges in CP and beyond CP	1401	Ground Floor Beams	Uniform distribution, mostly in beams
D-bracing-1600-0,1	No Performance Point	No Performance Point	721	381	305	100	No performance points, very high damage	1507	Ground Floor Columns	Spread across all stories
D-bracing-750-0,15	84,78	3101,0218	750	532	105	66	Higher hinge count, less effective	1453	Ground Floor Columns	Spread across all stories

D-bracing-1250-0,15	No Performance Point	No Performance Point	650	454	285	98	No performance points, high damage	1487	Ground Floor Columns	Spread across all stories
D-bracing-1600-0,15	97,361	3205,6449	803	511	4	0	Better performance, moderate hinges	1318	Second Floor Beams	Concentrated in lower and mid-levels

c. Inter-storey drift ratio

Inter-storey drift ratio is a critical measure of seismic performance, indicating potential damage during earthquakes. **Figures. 9-12** illustrate results for six-storey and nine-storey structures with X, V, and diagonal SMA bracing configurations, highlighting retrofitting strategies. Retrofitting with SMA bracings significantly reduces drift ratios to acceptable limits.

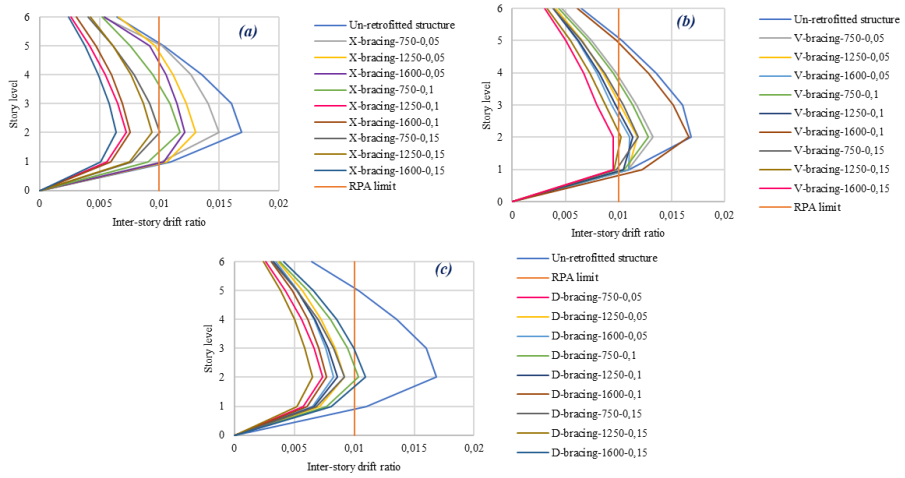


Figure. 9 *Inter-storey drift ratio for six-storey -X dir, a) X-bracing, b) V-bracing, and c) diagonal bracing.*

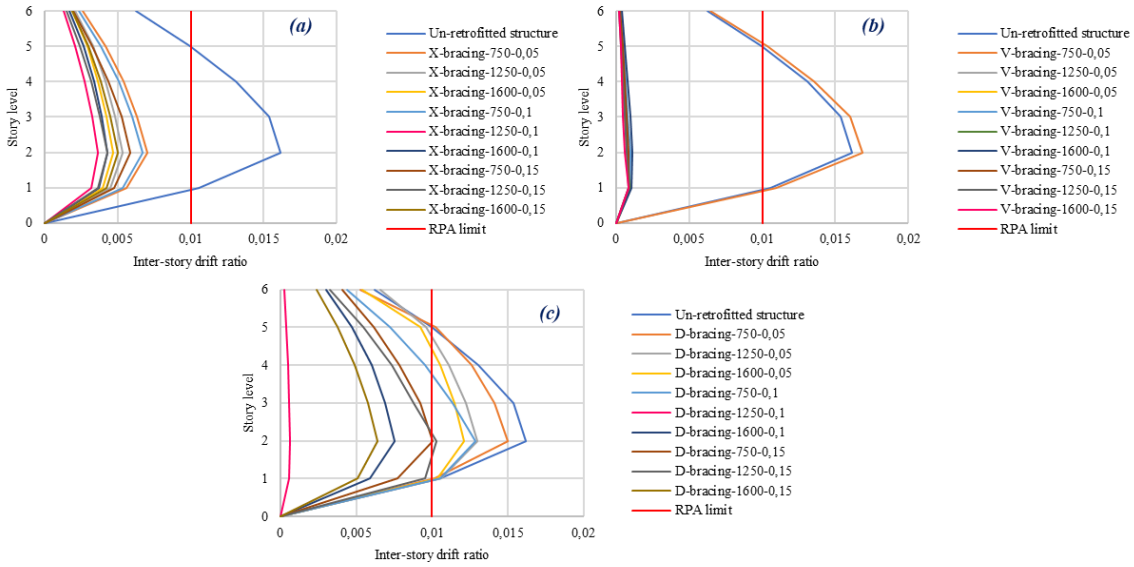


Figure. 10 Inter-storey drift ratio for six-storey -Y dir, a) X-bracing, b) V-bracing, and c) diagonal bracing.

For the six-storey structure, X-bracing (1250 mm², 0.1 damping) was the most effective, cutting the drift ratio by 60%. Its balance of stiffness and energy dissipation provided lateral stability and controlled displacements. V-bracing (1600 mm², 0.1 damping) reduced the drift ratio by 54% but concentrated forces at the base, making it less effective than X-bracing. Diagonal bracing achieved a 50% reduction, but performance varied due to less efficient force distribution.

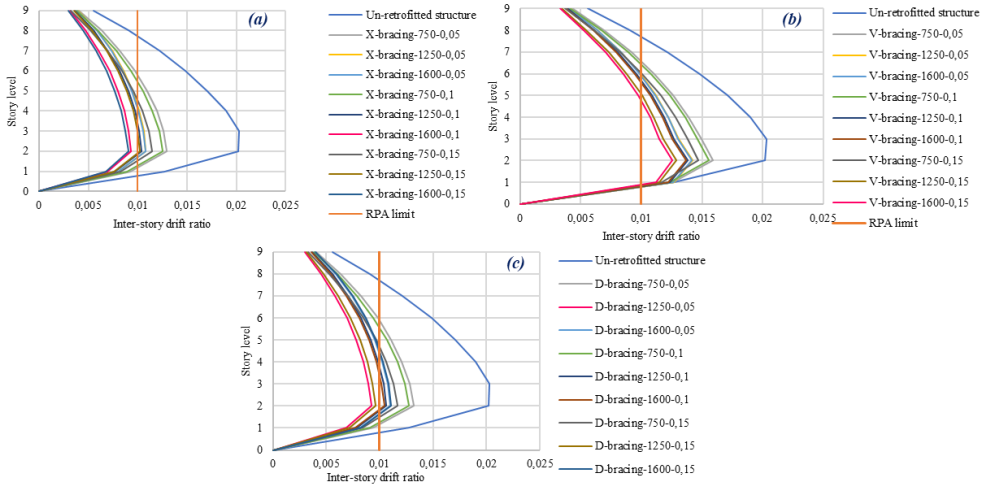


Figure. 11 *Inter-storey drift ratio for nine-storey -X dir, a) X-bracing, b) V-bracing, and c) diagonal bracing.*

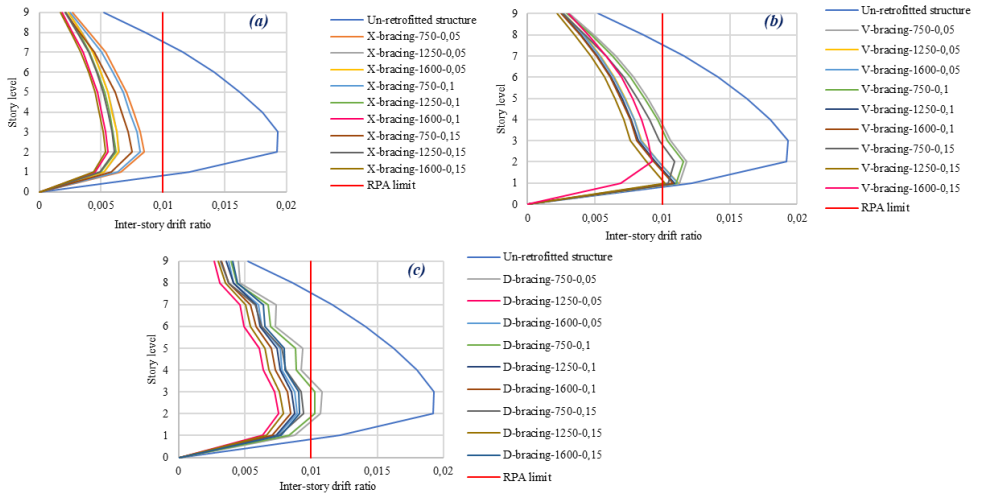


Figure. 12 *Inter-storey drift ratio for nine-storey -Y dir, a) X-bracing, b) V-bracing, and c) diagon al bracing*

For the nine-storey structure, X-bracing (1600 mm², 0.15 damping) reduced the maximum drift ratio by 56.8%, from 2.03% to 0.877%. The added stiffness and energy dissipation were crucial for controlling displacements in the taller structure. V-bracing and diagonal bracing also reduced drift ratios by 55.1% and 50%, respectively, but introduced more complex force paths, leading to variable performance in taller buildings.

d. Global ductility

Global ductility (μ) is essential for assessing a structure's deformability without significant strength loss, especially during seismic events. It is calculated as the design displacement (Δ_d) ratio to adjusted yield displacement ($\Delta_{y.Adj}$). Higher ductility indicates better energy absorption and dissipation, reducing the risk of failure. Ductility results for various bracing configurations and damping ratios in six-storey and nine-storey structures are summarized in **tables 12** through **23** for both X and Y directions.

The un-retrofitted six-storey structure shows low ductility (μ = 1.23), underscoring its limited capacity for inelastic deformation. X-bracing (1250 mm²,0.1 damping) improves ductility by 61% (μ = 1.98), providing an optimal balance of stiffness and flexibility. V-bracing (1600 mm²,0.15 damping) achieves the highest ductility at 2.07 (69% increase), thanks to its large cross-sections and high damping. In contrast, overly stiff configurations like V-bracing1(250 mm²,0.1 damping) (μ = 0.59) reduce ductility by 52%, limiting energy dissipation. D-bracing (750 mm²,0.05 damping) shows a remarkable 347% increase in ductility (μ = 5.49), demonstrating excellent flexibility, though with potentially excessive deformations.

Table 12 *Global Ductility of six-storey Structure with X-Bracing Configurations in the X Direction*

Case	Δ_d (mm)	Δ_{SMAB} (mm)	Δ_y (mm)	$\Delta_{y.Adj}$ (mm)	μ
Un-retrofitted structure	68.25	/	54.169	55.621	1.22705453
X-bracing-750-0.05	68.25	1.452	72.048	73.5	0.928571429
X-bracing-1250-0.05	68.25	1.452	57.353	58.805	1.160615594
X-bracing-1600-0.05	68.25	1.452	41.539	42.991	1.587541578
X-bracing-750-0.1	68.25	1.452	69.772	71.224	0.958244412
X-bracing-1250-0.1	68.25	1.452	32.966	34.418	1.982974025
X-bracing-1600-0.1	68.25	1.452	53.907	55.359	1.232861865
X-bracing-750-0.15	68.25	1.452	75.516	76.968	0.886732148
X-bracing-1250-0.15	68.25	1.452	61.355	62.807	1.086662315
X-bracing-1600-0.15	68.25	1.452	49.722	51.174	1.333685074

Table 13 *Global Ductility of six-storey Structure with V-Bracing Configurations in the X Direction*

Case	Δ_d(mm)	Δ_{SMAB}(mm)	Δ_y(mm)	$\Delta_{y.Adj}$ (mm)	μ
Un-retrofitted structure	68.25	/	54.169	55.621	1.22705453
V-bracing-750-0.05	68.25	1.452	59.376	60.828	1.122016177
V-bracing-1250-0.05	68.25	1.452	92.632	32.922	0.725415586
V-bracing-1600-0.05	68.25	1.452	60.799	62.251	1.09636793
V-bracing-750-0.1	68.25	1.452	36.356	37.808	1.805173508
V-bracing-1250-0.1	68.25	1.452	114.129	115.581	0.590494978
V-bracing-1600-0.1	68.25	1.452	50.316	51.768	1.318382012
V-bracing-750-0.15	68.25	1.452	82.03	83.482	0.817541506
V-bracing-1250-0.15	68.25	1.452	57.418	58.87	1.159334126
V-bracing-1600-0.15	68.25	1.452	31.47	94.084	2.07308183

Table 14 *Global Ductility of six-storey Structure with Diagonal-Bracing Configurations in the X Direction*

Case	Δ_d(mm)	Δ_{SMAB}(mm)	Δ_y(mm)	$\Delta_{y.Adj}$ (mm)	μ
Un-retrofitted structure	68.25	1.452	54.169	55.621	1.22705453
D-bracing-750-0.05	68.25	1.452	10.983	12.435	5.48854041
D-bracing-1250-0.05	68.25	1.452	49.553	51.005	1.338104107
D-bracing-1600-0.05	68.25	1.452	70.982	72.434	0.942237071
D-bracing-750-0.1	68.25	1.452	74.448	75.9	0.899209486
D-bracing-1250-0.1	68.25	1.452	55.882	57.334	1.190393135
D-bracing-1600-0.1	68.25	1.452	87.765	89.217	0.764988735
D-bracing-750-0.15	68.25	1.452	83.455	84.907	0.803820651
D-bracing-1250-0.15	68.25	1.452	58.864	60.316	1.131540553
D-bracing-1600-0.15	68.25	1.452	51.197	52.649	1.296320918

In the Y direction, the un-retrofitted six-storey structure has even lower ductility (μ = 0.62). X-bracing (1250 mm²,0.1 damping) improves this by 284% (μ = 2.38), while V-bracing (1600 mm²,0.1 damping) shows a more modest 33% increase (μ = 0.82). D-bracing (750 mm²,0.05 damping) increases ductility by 318% (μ = 2.59), indicating diagonal bracing's versatility.

Table 15 *Global Ductility of six-storey Structure with X-Bracing Configurations in the Y Direction*

Case	Δ_d (mm)	Δ_{SMAB} (mm)	Δ_y(mm)	$\Delta_{y.Adj}$ (mm)	μ
Un-retrofitted structure	68.25	1.452	54.169	55.621	1.22705453
X-bracing-750-0.05	68.25	1.452	72.048	73.5	0.928571429
X-bracing-1250-0.05	68.25	1.452	57.353	58.805	1.160615594
X-bracing-1600-0.05	68.25	1.452	41.539	42.991	1.587541578
X-bracing-750-0.1	68.25	1.452	69.772	71.224	0.958244412
X-bracing-1250-0.1	68.25	1.452	32.966	34.418	1.982974025
X-bracing-1600-0.1	68.25	1.452	53.907	55.359	1.232861865
X-bracing-750-0.15	68.25	1.452	75.516	76.968	0.886732148
X-bracing-1250-0.15	68.25	1.452	61.355	62.807	1.086662315
X-bracing-1600-0.15	68.25	1.452	49.722	51.174	1.333685074

Table 16 Global Ductility of Six-storey Structure with V-Bracing Configurations in the Y Direction

Case	Δ_d(mm)	Δ_{SMAB}(mm)	Δ_y(mm)	$\Delta_{y.Adj}$ (mm)	μ
Un-retrofitted structure	68.25	1.452	109.29	110.742	0.61629734
V-bracing-750-0.05	68.25	1.452	89.647	91.099	0.749184953
V-bracing-1250-0.05	68.25	1.452	79.975	81.427	0.83817407
V-bracing-1600-0.05	68.25	1.452	85.536	86.988	0.784590978
V-bracing-750-0.1	68.25	1.452	85.795	87.247	0.782261854
V-bracing-1250-0.1	68.25	1.452	81.565	83.017	0.82212077
V-bracing-1600-0.1	68.25	1.452	82.185	83.637	0.8160264

V-bracing-750-0.15	68.25	1.452	79.399	80.851	0.844145403
V-bracing-1250-0.15	68.25	1.452	79.935	81.387	0.838586015
V-bracing-1600-0.15	68.25	1.452	48.892	50.344	1.35567297

Table 17 *Global Ductility of six-storey Structure with Diagonal-Bracing Configurations in the Y Direction*

Case	Δ_d(mm)	Δ_{SMAB}(mm)	Δ_y(mm)	$\Delta_{y.Adj}$ (mm)	μ
Un-retrofitted structure	68.25	1.452	109.29	110.742	0.61629734
D-bracing-750-0.05	68.25	1.452	24.928	26.38	2.587187263
D-bracing-1250-0.05	68.25	1.452	82.517	83.969	0.812799962
D-bracing-1600-0.05	68.25	1.452	71.049	72.501	0.941366326
D-bracing-750-0.1	68.25	1.452	71.629	73.081	0.933895267
D-bracing-1250-0.1	68.25	1.452	66.38	67.832	1.006162283
D-bracing-1600-0.1	68.25	1.452	49.376	50.828	1.342763831
D-bracing-750-0.15	68.25	1.452	77.55	79.002	0.86390218
D-bracing-1250-0.15	68.25	1.452	64.871	66.323	1.029054777
D-bracing-1600-0.15	68.25	1.452	61.896	63.348	1.07738208

For the nine-storey structure, the un-retrofitted ductility is low (μ = 0.85). X-bracing (1600 mm²,0.1 damping) improves it by 21% (μ = 1.03), showing moderate gains from large cross-sections and damping. V-bracing (1600 mm²,0.15 damping) significantly boosts ductility by 220% (μ = 2.72), reflecting excellent energy dissipation. D-bracing (1250 mm²,0.05 damping) shows a 96% increase (μ = 1.67), indicating diagonal bracing's effectiveness when optimally configured.

Table 18 *Global Ductility of nine-storey Structure with X-Bracing Configurations in the X Direction.*

Case	Δ_d(mm)	Δ_{SMAB}(mm)	Δ_y(mm)	$\Delta_{y.Adj}$ (mm)	μ
Un-retrofitted structure	68.25	1.452	78.84	80.292	0.850022418
X-bracing-750-0.05	68.25	1.452	92.095	93.547	0.729579783
X-bracing-1250-0.05	68.25	1.452	91.056	92.508	0.73777403
X-bracing-1600-0.05	68.25	1.452	94.919	96.371	0.7082006
X-bracing-750-0.1	68.25	1.452	86.546	87.998	0.775585809
X-bracing-1250-0.1	68.25	1.452	82.717	84.169	0.81086861
X-bracing-1600-0.1	68.25	1.452	64.797	66.249	1.030204229
X-bracing-750-0.15	68.25	1.452	92.08	93.532	0.729696788
X-bracing-1250-0.15	68.25	1.452	82.028	83.48	0.817561092
X-bracing-1600-0.15	68.25	1.452	75.118	76.57	0.891341256

Table 19 *Global Ductility of nine-storey Structure with V-Bracing Configurations in the X Direction*

Case	Δ_d(mm)	Δ_{SMAB}(mm)	Δ_y(mm)	$\Delta_{y.Adj}$ (mm)	μ
Un-retrofitted structure	68.25	1.452	78.84	80.292	0.850022418
V-bracing-750-0.05	68.25	1.452	87.707	89.159	0.765486378
V-bracing-1250-0.05	68.25	1.452	59.368	60.82	1.122163762
V-bracing-1600-0.05	68.25	1.452	60.62	62.072	1.099529579
V-bracing-750-0.1	68.25	1.452	60.579	62.031	1.100256323
V-bracing-1250-0.1	68.25	1.452	59.113	60.565	1.126888467
V-bracing-1600-0.1	68.25	1.452	58.96	60.412	1.129742435
V-bracing-750-0.15	68.25	1.452	62.845	64.297	1.061480318
V-bracing-1250-0.15	68.25	1.452	60.097	61.549	1.108872606
V-bracing-1600-0.15	68.25	1.452	5.089	25.052	2.724333387

Table 20 *Global Ductility of nine-storey Structure with Diagonal-Bracing Configurations in the X Direction*

Case	Δ_d(mm)	Δ_{SMAB}(mm)	Δ_y(mm)	$\Delta_{y.Adj}$ (mm)	μ
Un-retrofitted structure	68.25	1.452	78.84	80.292	0.850022418
D-bracing-750-0.05	68.25	1.452	70.806	72.258	0.944532093
D-bracing-1250-0.05	68.25	1.452	39.393	40.845	1.670951157
-bracing-1600-0.05	68.25	1.452	70.603	72.055	0.947193116
D-bracing-750-0.1	68.25	1.452	90.73	92.182	0.740383155
D-bracing-1250-0.1	68.25	1.452	82.093	83.545	0.81692501
D-bracing-1600-0.1	68.25	1.452	70.352	71.804	0.95050415
D-bracing-750-0.15	68.25	1.452	71.131	72.583	0.940302826
D-bracing-1250-0.15	68.25	1.452	70.488	71.94	0.948707256
D-bracing-1600-0.15	68.25	1.452	71.809	73.261	0.931600715

In the Y direction, the un-retrofitted nine-storey structure has very low ductility (μ = 0.57). X-bracing (1600 mm²,0.1 damping) improves it by 267% (μ = 2.10), while other X-bracing configurations show increases between 42% and 105%. V-bracing configurations generally

fall below 1.0, with V-bracing (1600 mm²,0.1 damping) showing a 35% increase (μ = 0.77). D-bracing (1250 mm²,0.05 damping) improves ductility by 145% (μ = 1.40), demonstrating the potential of diagonal bracing in enhancing ductility with proper setup.

Table 21 *Global Ductility of nine-storey Structure with X-Bracing Configurations in the Y Direction*

Case	Δ_d(mm)	Δ_{SMAB}(mm)	Δ_y(mm)	$\Delta_{y.Adj}$ (mm)	μ
Un-retrofitted structure	68.25	1.452	117.705	119.157	0.572773735
X-bracing-750-0.05	68.25	1.452	79.306	80.758	0.845117512
X-bracing-1250-0.05	68.25	1.452	68.774	70.226	0.971862273
X-bracing-1600-0.05	68.25	1.452	74.534	75.986	0.898191772
X-bracing-750-0.1	68.25	1.452	73.893	75.345	0.905833167
X-bracing-1250-0.1	68.25	1.452	68.445	69.897	0.976436757
X-bracing-1600-0.1	68.25	1.452	31.007	32.459	2.102652577
X-bracing-750-0.15	68.25	1.452	82.54	83.992	0.812577388
X-bracing-1250-0.15	68.25	1.452	67.829	69.281	0.985118575
X-bracing-1600-0.15	68.25	1.452	61.714	63.166	1.080486338

Table 22 *Global Ductility of NINE-STOREY Structure with V-Bracing Configurations in the Y Direction.*

Case	Δ_d(mm)	Δ_{SMAB}(mm)	Δ_y(mm)	$\Delta_{y.Adj}$ (mm)	μ
Un-retrofitted structure	68.25	1.452	117.705	119.157	0.572773735
V-bracing-750-0.05	68.25	1.452	85.107	86.559	0.788479534
V-bracing-1250-0.05	68.25	1.452	86.715	88.167	0.774099153
V-bracing-1600-0.05	68.25	1.452	85.684	87.136	0.783258355
V-bracing-750-0.1	68.25	1.452	85.637	87.089	0.783681062
V-bracing-1250-0.1	68.25	1.452	86.204	87.656	0.778611846
V-bracing-1600-0.1	68.25	1.452	87.155	88.607	0.770255172
V-bracing-750-0.15	68.25	1.452	84.442	85.894	0.794584022
V-bracing-1250-0.15	68.25	1.452	86.912	88.364	0.772373365
V-bracing-1600-0.15	68.25	1.452	59.046	60.498	1.128136467

Table 23 *Global Ductility of nine-storey Structure with Diagonal-Bracing Configurations in the Y Direction*

Case	Δ_d(mm)	Δ_{SMAB}(mm)	Δ_y(mm)	$\Delta_{y.Adj}$ (mm)	μ
Un-retrofitted structure	68.25	1.452	117.705	119.157	0.572773735
D-bracing-750-0.05	68.25	1.452	76.884	78.336	0.871246936
D-bracing-1250-0.05	68.25	1.452	47.228	48.68	1.402013147
D-bracing-1600-0.05	68.25	1.452	63.252	64.704	1.054803412
D-bracing-750-0.1	68.25	1.452	66.172	67.624	1.009257068
D-bracing-1250-0.1	68.25	1.452	58.973	60.425	1.129499379
D-bracing-1600-0.1	68.25	1.452	62.152	63.604	1.07304572
D-bracing-750-0.15	68.25	1.452	69.494	70.946	0.961999267
D-bracing-1250-0.15	68.25	1.452	65.836	67.288	1.014296754
D-bracing-1600-0.15	68.25	1.452	74.128	75.58	0.903016671

4.2 Summary and Conclusions from Pushover Analysis Results

The pushover analysis conducted on six-storey and nine-storey RC structures retrofitted with SMA bracing configurations offers critical insights into optimising seismic performance. For the six-storey structure, the retrofitting measures yielded significant improvements in structural capacity, reduced inter-storey drifts, and enhanced global ductility. Notably, the X-bracing configuration with a cross-sectional area of 1250 mm² and a damping ratio of 0.1 emerged as the optimal solution, achieving a precise balance between stiffness and flexibility. This configuration minimised plastic hinge formation, predominantly maintaining the Immediate Occupancy and Life Safety performance levels while significantly reducing displacements at the performance point. Similarly, the nine-storey structure exhibited notable improvements when retrofitted with X-bracing of 1600 mm² cross-sectional area and 0.1 damping ratio, leading to better displacement control, lower drift ratios, and improved ductility. These findings underscore the decisive role of carefully selected bracing configurations in enhancing seismic resilience. To further solidify these outcomes, the most promising configurations will undergo rigorous evaluation through NLTHA, ensuring their effectiveness under actual seismic conditions and establishing their potential to bolster structural safety significantly.

4.3 Nonlinear time history analysis results

To further verify and supplement the findings from the pushover analysis, NLTHA was conducted on the six-storey and nine-storey structures, using seven matched earthquake records and their matched mean spectrum. This step aims to validate the performance

improvements observed after retrofitting, as assessed in Scenario 5, and to evaluate the dynamic response of both the un-retrofitted and retrofitted structures under actual seismic conditions. The analysis focused on crucial response metrics, including peak floor accelerations, residual displacements, and displacement profiles.

4.3.1 Peak Floor Acceleration (PFA)

Peak Floor Acceleration (PFA) is a critical metric for assessing seismic demand on each floor during an earthquake, providing valuable insights into the dynamic behaviour of the retrofitted and un-retrofitted structures.

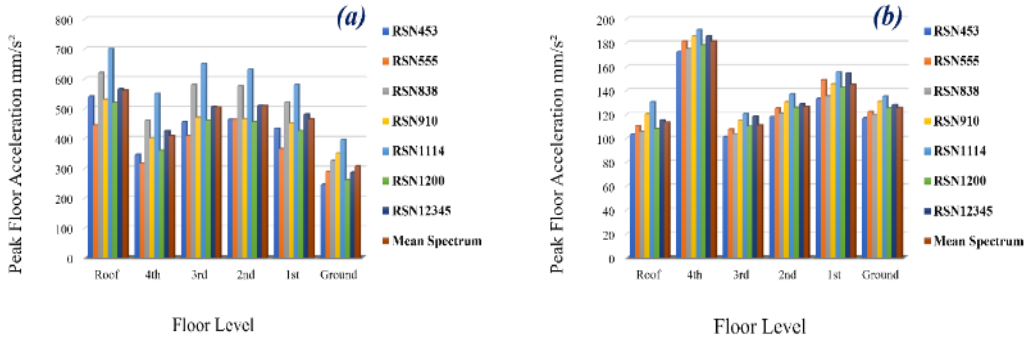


Figure. 13 *Peak floor acceleration for six-storey, a) Un-retrofitted structure, b) retrofitted structure*

The results of the un-retrofitted six-storey structure (**Figure. 13.a**) show significantly elevated accelerations on the upper floors, exceeding 600 mm/s² for seismic records like RSN838 and RSN1114. This high acceleration reflects the structure's inadequate lateral stiffness and limited global ductility, as previously highlighted in the pushover analysis. The highest accelerations occur at the roof, indicating insufficient energy dissipation, as evidenced by plastic hinge formations in the upper stories. In contrast, the retrofitted six-storey structure (**Figure. 13.b**) dramatically reduces peak accelerations, falling below 150 mm/s² on all floors, even under the most intense seismic loads. This improvement, linked to increased stiffness and strength from retrofitting, results in a more uniform and controlled response across all floors, showcasing better force distribution and enhanced damping capacity.

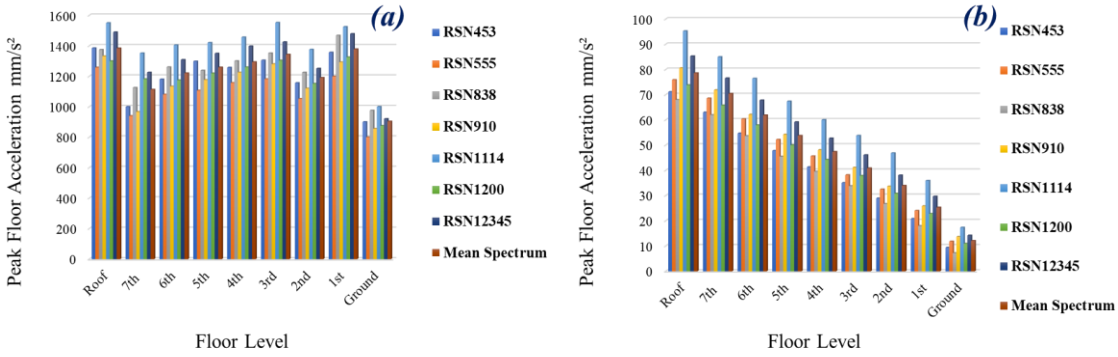


Figure. 14 *Peak floor acceleration for nine-storey, a) Un-retrofitted structure, b) retrofitted structure*

Similarly, for the nine-storey structure, the un-retrofitted PFA results (**Figure. 14.a**) reveal pronounced seismic vulnerability, with the roof experiencing an average PFA of 1384.72 mm/s², peaking at 1550.59 mm/s² under record RSN1114. Even the lower floors demonstrate substantial accelerations, with the ground floor reaching 904.27 mm/s². These high values highlight the structure's insufficient seismic resistance, which aligns with the pushover analysis, indicating low base shear capacity and early plastic hinge formation. After retrofitting with X-bracing (1600 mm², 0.1 damping) (**Figure. 14.b**), the seismic performance improves significantly, with the roof-level PFA dropping by over 94%, from 1384.72 mm/s² to just 78.58 mm/s². Lower floors also experience significant reductions, such as the 7th floor's drop to 70.41 mm/s² and the ground floor's reduction to 12.08 mm/s². These improvements confirm the enhanced lateral stiffness, base shear resistance, and energy dissipation achieved through retrofitting.

The significant reduction in PFA across all floors, with reductions between 80% and 94%, demonstrates that retrofitting increases the

structure's lateral load capacity and ensures a more uniform distribution of seismic forces, effectively protecting both upper and lower stories from excessive acceleration levels.

4.3.2 Residual displacement

Residual displacement represents the permanent deformation of structural members following seismic events, indicating the extent of irrecoverable damage. In this analysis, **Figures 15a** and **15b** illustrate the residual displacements for the un-retrofitted six-storey structure in the X and Y directions, respectively. **Figures 16a** and **16b** display the corresponding results for the retrofitted structure.

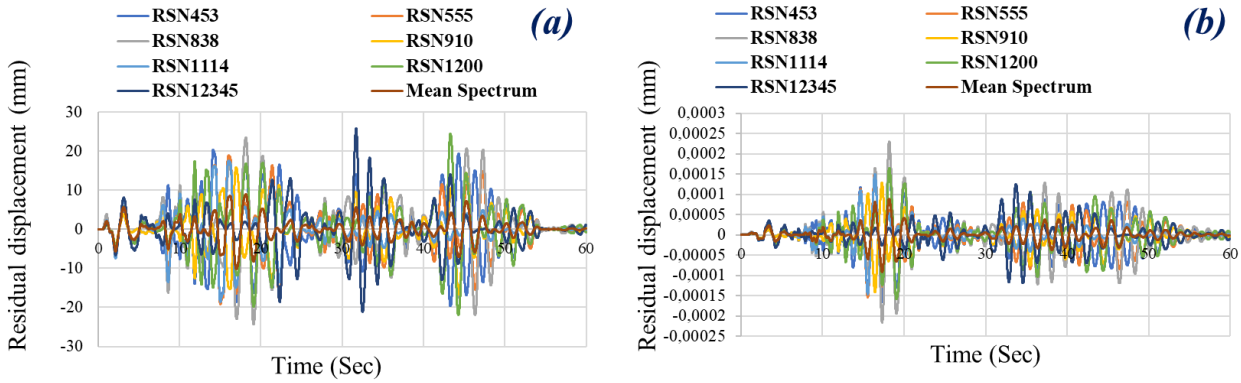


Figure. 15 *Residual Displacement Time-History for the Un-Retrofitted six-storey Structure in X -a) and Y -b) Directions*

In the un-retrofitted structure, large residual displacements occur in both directions, indicating poor seismic performance, low stiffness, and limited post-yield strength. These deformations align with the pushover analysis, which revealed early hinge formation and inadequate lateral load-bearing capacity, especially in the upper stories.

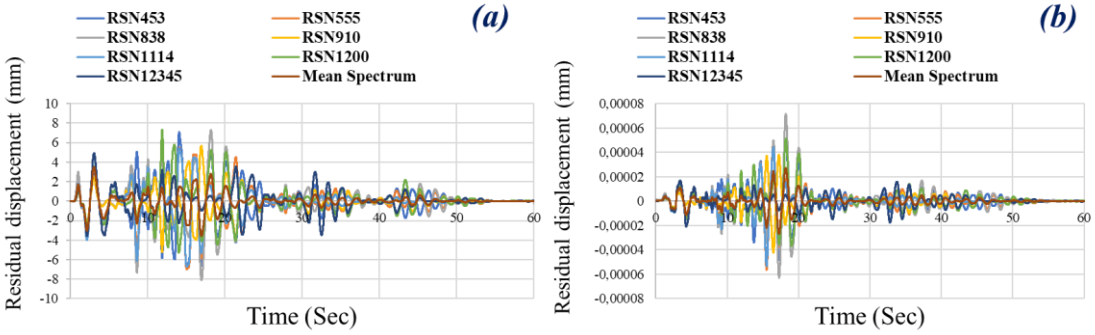


Figure. 16 *Residual Displacement Time-History for the Retrofitted six-storey Structure in X -a) and Y -b) Directions*

After retrofitting with X-bracing (1250 mm², 0.1 damping), residual displacements in the X direction drop by 94%, showing much better control and minimal permanent deformation post-earthquake. As the pushover analysis shows, the structure exhibits enhanced stiffness and energy dissipation. In the Y direction, displacements are reduced by 95%, although there's slightly more variability than in the X direction. Retrofitting significantly improves seismic resilience, reducing permanent damage and better distributing seismic forces.

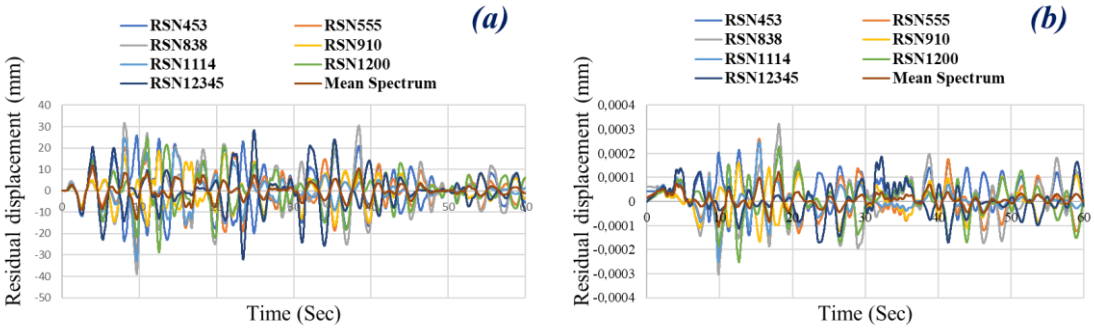


Figure. 17 *Residual Displacement Time-History for the Un-Retrofitted nine-storey Structure in X -a) and Y -b)*

Directions

The un-retrofitted nine-storey structure exhibits significant residual displacements, as seen in **Figure 17**. In the X direction (**Figure 17a**), displacements peak at 30 mm, while in the Y direction (**Figure 17b**), they reach around 0.0003 mm. These large deformations highlight the structure's inability to dissipate energy effectively, with poor stiffness and ductility, as reflected in early hinge formation from the pushover analysis. The structure struggles to redistribute seismic forces, resulting in excessive inelastic deformation.

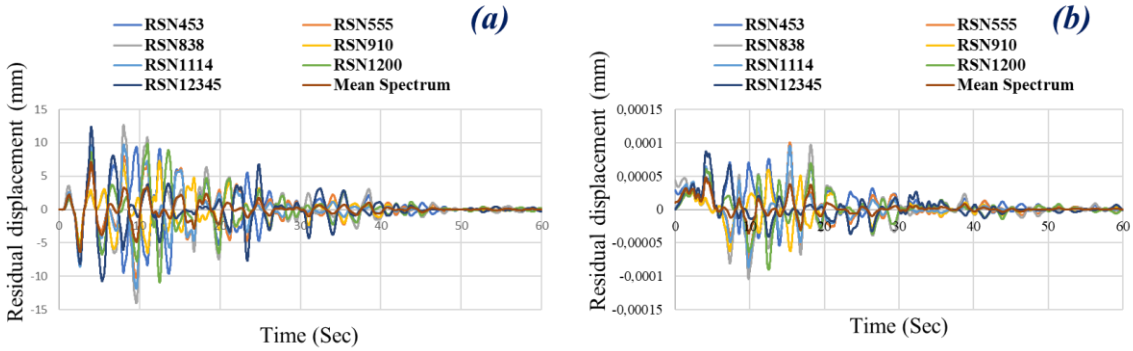


Figure. 18 *Residual Displacement Time-History for the Retrofitted NINE-STOREY Structure in X -a) and Y - b) Directions*

After retrofitting, the residual displacements drop dramatically, as shown in **Figure 18**. In the X direction (**Figure 18a**), the displacements decrease by 63%, from 30 mm to around 11 mm, while in the Y direction (**Figure 18b**), the displacement further reduces to an almost negligible 0.0001 mm. The displacement-time histories show more controlled, damped responses with minimal permanent deformations. The X-bracing system significantly enhances stiffness, delays hinge formation, and improves lateral load capacity, aligning with the pushover results. This underscores the retrofitting's effectiveness in improving seismic resilience and reducing permanent structural damage.

4.3.3 Displacement profiles

Figure 19a illustrates the displacement profile of the un-retrofitted six-storey structure across various seismic records. The un-retrofitted structure shows more enormous inter-storey drifts, particularly at the upper stories, with displacements reaching up to 0.35m. This suggests a higher vulnerability to excessive deformation and potential structural damage. **Figure 19b**, representing the retrofitted six-storey structure, shows a significant displacement across all stories. The peak displacement in the retrofitted structure drops to approximately 0.025m, indicating a reduction of 93% in overall displacement compared to the un-retrofitted case. The effect of the retrofitting method, which included X-bracing with a 1250 mm², 0.1 damping, is visible here. The X-bracing enhances lateral stiffness, controlling storey drifts and improving structural resilience under seismic loads. This aligns with the results from the pushover analysis, where the retrofitted six-storey structure showed improved performance with reduced base shear and roof displacement.

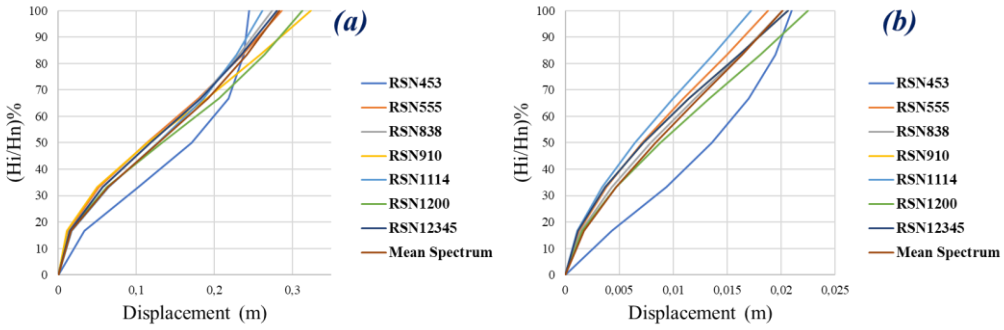


Figure. 19 *Displacement Profile of six-storey Structure, a) Un-retrofitted, b) Retrofitted*

Figure 20a shows the displacement profile of the un-retrofitted nine-storey structure. Similarly to the six-storey structure, the un-retrofitted nine-storey shows substantial storey drifts, with displacements reaching over 0.50m in the upper stories. This suggests even greater

susceptibility to lateral loads due to the taller configuration. **Figure 20b** presents the displacement profile of the retrofitted nine-storey structure. The retrofitting significantly reduces the maximum displacement to around 0.1m, representing a reduction of about 80% compared to the un-retrofitted structure. This result also demonstrates the effectiveness of the retrofitting method in tall structures. The X-bracing for the nine-storey significantly improves the performance by enhancing lateral stiffness, minimising inter-storey drifts, and reducing overall displacement. This is consistent with the observations from the PFA results, where the retrofitted nine-storey structure experienced lower floor accelerations compared to the un-retrofitted one, as well as the residual displacement results, which confirmed that retrofitting reduced the permanent deformations in the structure.

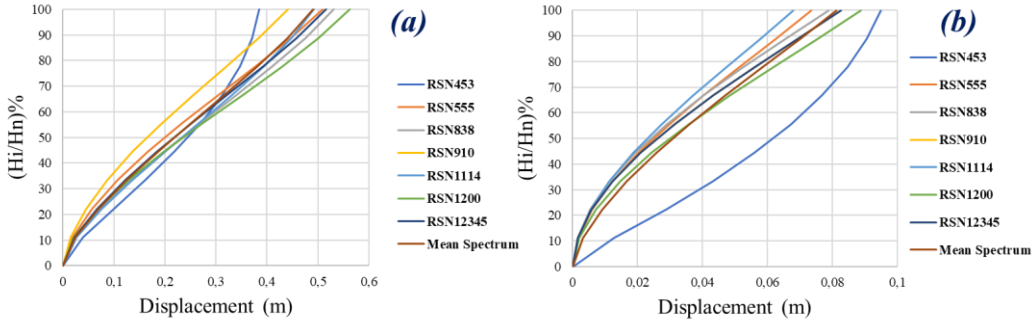


Figure. 20. *Displacement Profile of nine-storey Structure, a) Un-retrofitted, b) Retrofitted*

5. Comparative Performance Analysis of SMA and Steel Bracings in Seismic Retrofitting

In this section, we conduct a comparative analysis of SMA and traditional steel bracings to evaluate their performance in seismic retrofitting. The objective is to verify the advantages of SMA bracings, particularly in terms of residual displacements, energy dissipation, and global ductility. By comparing these two systems, we aim to demonstrate the potential of SMA bracings as a superior solution for enhancing the seismic resilience of non-compliant reinforced concrete (RC) structures.

5.1 Properties of Steel Bracings

The steel bracing system chosen for this analysis is the X-bracing configuration, known for its effectiveness in providing higher lateral stability and energy dissipation during seismic events. The findings of Tahamouli Roudsari et al support the choice of X-bracing. [29], who experimentally assessed various bracing systems for retrofitting RC frames. The properties used in this analysis are summarised in **Table 24**.

Table 24 *Properties of Steel X-Bracings Used in the Numerical Analysis.*

Property	value
Yield Strength	328.2 MPa (Flange), 332.7 MPa (Web)
Tensile Strength	493 MPa (Flange), 478 MPa (Web)
Elastic Modulus	197 GPa (Flange), 195 GPa (Web)
Cross-sectional Area	IPE140: 1706.4 mm²
Moment of Inertia (I_{xx})	191.9 × 10⁶ mm⁴ (191.9 cm⁴)
Damping Properties	2%
Load-Displacement Behaviour	Hysteresis behaviour from cyclic loading [29]

5.2 Results and Discussion

This study employed Pushover Analysis as a simplified yet effective method to evaluate the seismic performance of SMA and steel bracings in retrofitting RC structures. By gradually applying lateral loads, Pushover Analysis provides valuable insights into the structure's global behaviour, allowing us to assess key performance parameters such as residual displacement, inter-storey drift, and global ductility.

5.2.1 Residual Displacement

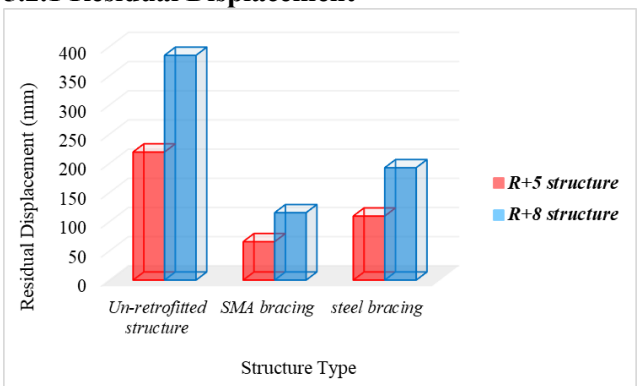


Figure. 21 Comparison of Residual Displacement for six-storey and nine-storey Structures

Figure 21 shows the residual displacement for six-storey and nine-storey structures in un-retrofitted, SMA-braced, and steel-braced scenarios. The un-retrofitted six-storey structure has a displacement of 219.53 mm, while the nine-storey structure shows 385.18 mm, indicating that taller buildings suffer greater deformation during seismic events. After retrofitting, SMA bracings reduce the displacement by 70% to 65.86 mm for the six-storey and 115.55 mm for the nine-storey. This is due to SMA's superelastic properties, which allow the structure to recenter after seismic loads. In comparison, steel bracings show a 50% reduction, lowering displacement to 109.76 mm for six-storey and 192.59 mm for nine-storey due to steel's tendency to yield under seismic stress, resulting in permanent deformation.

Generally speaking, SMA bracings are more effective in reducing residual displacement, making them a better option for seismic retrofitting than steel bracings.

5.2.2 Inter-Storey Drift Ratio

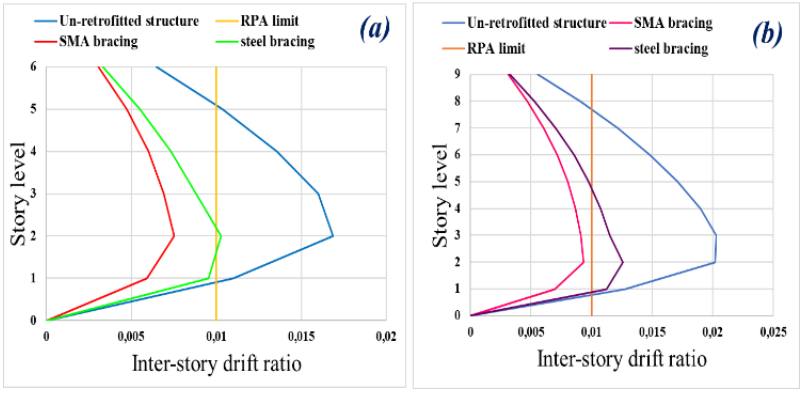


Figure. 22 *Inter-Storey Drift Ratios for a) six-storey, b) nine-storey Structures*

In both graphs, the un-retrofitted structures significantly exceed the RPA limit, particularly at mid and upper-storey levels. This indicates a high risk of damage, especially for the taller nine-storey structure, which has greater drift and is more vulnerable during seismic events. The SMA bracings significantly reduce the inter-storey drift ratios for both structures, keeping the values within the RPA safety limit across all stories. This shows the effectiveness of SMA bracings in controlling lateral displacements and protecting the structure from seismic damage, especially in taller buildings like nine-storey, where it brings the drift ratios close to zero. Steel bracings also reduce drift but are less effective than SMA. For the six-storey structure (**Figure 22a**), steel bracing brings the drift ratios near the RPA limit. In contrast, for the nine-storey structure (**Figure 22b**), steel bracings exceed the RPA limit at mid-levels, showing moderate improvement, but are less efficient in taller buildings.

5.2.3 Global Ductility Ratio

Table 7 *Comparison of Global Ductility Ratios for six-storey and nine-storey Structures*

Structure Type		Un-Retrofitted	SMA Bracing	Steel Bracing
SIX-STOREY	Global Ductility Ratio	1.22705453	1.65646544	1.41175998
NINE-STOREY	Global Ductility Ratio	0.850022418	1.19002690	1.02042466

The analysis of global ductility ratios demonstrates significant improvements in structural performance with both SMA and steel bracing systems, particularly for the nine-storey structure. Due to its superelastic properties and superior energy dissipation capacity, SMA bracing outperforms steel

bracing in enhancing ductility. For the six-storey structure, SMA bracing increases ductility by approximately 35% compared to the un-retrofitted state, while steel bracing provides a 15% improvement. The difference is more pronounced in the nine-storey structure. SMA bracing boosts ductility by about 40%, pushing it well above the critical value of 1 (from 0.85 to 1.19), indicating a substantial shift from brittle to ductile behaviour. In contrast, steel bracing increases nine-storey ductility by 20% (to 1.02), barely exceeding the ductility threshold 1. Notably, the taller nine-storey structure benefits more from bracing, with SMA offering a 100% greater improvement in ductility compared to steel bracing. These results validate the superior performance of SMA bracing, especially for taller structures, suggesting its potential for significantly enhanced seismic resilience and energy dissipation capacity in retrofitted buildings.

6 Conclusion

This study aimed to develop an innovative seismic retrofitting approach by integrating Shape Memory Alloy bracings into a Direct Displacement-Based Design framework tailored for non-compliant reinforced concrete structures. The research addressed seismic vulnerabilities by leveraging SMA bracings' unique properties, including superior energy dissipation and self-centring capabilities. Through both nonlinear static pushover and nonlinear time history analyses, the findings demonstrated that SMA bracings significantly improve seismic performance. Among the tested bracing configurations, the X-bracing system with a 1250 mm² cross-sectional area and a 0.1 damping ratio was identified as the optimal solution for mid-rise structures (six-storey). This configuration truly balanced stiffness and flexibility by reducing inter-storey drift by over 56% and improving energy dissipation during seismic events. For taller structures (nine-storey), the X-bracing system with a 1600 mm² cross-sectional area and a 0.1 damping ratio proved the most effective, reducing drift by nearly 57%. The damping ratio was appropriate for both structures, ensuring optimal energy absorption without compromising the system's structural integrity under seismic loads. The introduction of SMA bracings significantly enhanced the global ductility of both structures. In the six-storey structure, ductility improved by 69%, while the nine-storey structure saw a more than 50% improvement. These increases in ductility allow the structures to absorb and dissipate more seismic energy, reducing the risk of catastrophic failure. Importantly, the displacement profiles for both structures demonstrated that the retrofitted buildings could control their dynamic response far better than the un-retrofitted versions, with lateral displacements reduced by approximately 30%. This reduction indicates that the retrofitted structures were better equipped to resist seismic forces and maintain stability during an earthquake. Plastic hinge formation was also better controlled with SMA bracings, particularly at the CP level, where most plastic hinges remained within IO and LS performance levels. This shows that SMA bracings effectively prevent critical damage during strong seismic events, further improving the overall safety of retrofitted structures. Moreover, the residual displacements in the SMA-braced structures were reduced by over 85%, highlighting the exceptional re-centring ability of SMA. This reduction minimises post-seismic repairs and ensures quicker recovery after earthquakes. The Peak Floor Accelerations in the retrofitted buildings were reduced by over 90%, indicating that SMA bracings significantly improved the dynamic response of the structures and minimised the risk of structural and non-structural damage. The validation of SMA bracings' effectiveness was further confirmed by comparing them with steel bracings. SMA bracings reduced residual displacements by 70% in the six-storey structure and 63% in the nine-storey structure, whereas steel bracings achieved only a 50% reduction in both cases. Additionally, global ductility saw larger improvements with SMA bracings, enhancing ductility by 35% in six-storey and 40% in nine-storey, while steel bracings showed only moderate gains. These results validate the superior performance of SMA bracings in controlling deformations and ensuring the structure can return to its original position with minimal permanent damage. The superelastic properties of SMA provide better recentering capability and ensure greater resilience compared to traditional steel bracings, which are more prone to yielding and permanent deformation under seismic loads.

Although this study focused on specific mid- and high-rise structures in Algeria, the findings can be generalised globally to a wider range of low-, medium-, and high-rise structures. SMA bracings can be applied effectively in various seismic regions,

offering a scalable and adaptable solution to improve seismic performance. Their ability to minimise permanent deformations, improve structural recovery, and reduce repair costs makes them a valuable tool in retrofitting RC buildings worldwide, ensuring compliance with both local and international seismic codes.

In conclusion, this research demonstrates that integrating SMA bracings into the DDBD framework provides a cost-effective, scalable, and adaptable method for improving the seismic resilience of non-compliant RC structures. Future studies should explore the broader application of this retrofitting approach to steel, hybrid structures, and low-rise buildings in urban and rural settings. Furthermore, analysing the long-term efficacy of SMA bracings under recurrent earthquake occurrences and severe environmental events would further substantiate their reliability. Advanced simulations, including machine learning-based prediction models, may enhance the optimisation of SMA bracing design for a broader spectrum of buildings and seismic intensities, aiding worldwide initiatives in earthquake hazard reduction.

Author Statements:

- **Ethical approval:** The conducted research is not related to either human or animal use.
- **Conflict of interest:** The authors declare that they have no known competing financial interests or personal relationships that could have appeared to influence the work reported in this paper.
- **Acknowledgement:** The authors would like to acknowledge the support and resources provided by the Civil Engineering and Hydraulic Laboratory at the University of 8 Mai 1945, Guelma, Algeria, in conducting this research.
- **Author contributions:** The authors declare that they have equal rights on this paper.
- **Funding information:** The authors declare that there is no funding to be acknowledged.
- **Data availability statement:** The data that support the findings of this study are available on request from the corresponding author. The data are not publicly available due to privacy or ethical restrictions.

References

[1] Algériennes, R.P. (2003). RPA 99/Version 2003, Cent. Natl. Rech. Apliquée En Génie Parasismique, Algiers, Alger., ,.

[2] Qian, H., Li, H., Song, G. (2016). Experimental investigations of building structure with a superelastic shape memory alloy friction damper subject to seismic loads, Smart Mater. Struct., 25(12), pp. 125026.

[3] Wang, B., Zhu, S. (2018). Seismic behavior of self-centering reinforced concrete wall enabled by superelastic shape memory alloy bars, Bull. Earthq. Eng., 16, pp. 479–502.

[4] Kari, A., Ghassemieh, M., Abolmaali, S.A. (2011). A new dual bracing system for improving the seismic behavior of steel structures, Smart Mater. Struct., 20(12), pp. 125020.

[5] Miller, D.J., Fahnestock, L.A., Eatherton, M.R. (2012). Development and experimental validation of a nickel–titanium shape memory alloy self-centering buckling-restrained brace, Eng. Struct., 40, pp. 288–98.

[6] Moradi, S., Alam, M.S., Asgarian, B. (2014). Incremental dynamic analysis of steel frames equipped with NiTi shape memory alloy braces, Struct. Des. Tall Spec. Build., 23(18), pp. 1406–25.

[7] Asgarian, B., Moradi, S. (2011). Seismic response of steel braced frames with shape memory alloy braces, J. Constr. Steel Res., 67(1), pp. 65–74.

[8] Ferraioli, M., Concilio, A., Molitierno, C. (2022). Seismic performance of a reinforced concrete building retrofitted with self-centering shape memory alloy braces, Earthq. Eng. Eng. Vib., 21(3), pp. 785–809.

[9] Ferraioli, M., Lavino, A. (2018). A displacement-based design method for seismic retrofit of RC buildings using dissipative braces, Math. Probl. Eng., 2018, pp. 1–28.

[10] Miani, M. (2021). INNOVATIVE SEISMIC PROTECTION OF EXISTING BUILDINGS BY MEANS OF DISSIPATIVE AND SHAPE MEMORY ALLOY BRACES, ,.

[11] Abraik, E., Asif, I. (2023). A comparison of utilization design ratios of self-centering shape memory alloy with different brace configurations, Eng. Struct., 281, pp. 115768.

[12] Vignoli, L.L., Savi, M.A., El-Borgi, S. (2020). Nonlinear dynamics of earthquake-resistant structures using shape memory alloy composites, J. Intell. Mater. Syst. Struct., 31(5), pp. 771–87.

[13] Matari, Z., Bourdim, S.M.E.-A., Rodrigues, H., Kadri, T. (2023). Earthquake Analysis of an Old RC Minaret Retrofitting with Shape Memory Alloy, Buildings, 13(5), pp. 1121.

[14] Calvi, G.M., Priestley, M.J.N., Kowalsky, M.J. (2008). Displacement – Based Seismic Design of Structures, ,.

[15] Bergami, A.V., Nuti, C. (2013). A design procedure of dissipative braces for seismic upgrading structures, Earthquakes Struct., 4(1), pp. 85–108.

[16] Mazza, F., Vulcano, A. (2014). Equivalent viscous damping for displacement-based seismic design of hysteretic damped braces for retrofitting framed buildings, Bull. Earthq. Eng., 12, pp. 2797–819.

[17] Mazza, F. (2014). Displacement-based seismic design of hysteretic damped braces for retrofitting in-plan irregular rc framed structures, Soil Dyn. Earthq. Eng., 66, pp. 231–40.

[18] Monti, G., Rabi, R.R., Vailati, M. (2024). Direct displacement-based design of dissipative bracings for seismic retrofit of reinforced concrete buildings, J. Build. Eng., 82, pp. 108208.

[19] Alehojjat, S.B., Yakhchalian, M., Bahar, O. (2023). Approximate methods to estimate residual drift demands in steel structures with viscous dampers designed by the DDBD approach, Int. J. Steel Struct., 23(3), pp. 806–22.

[20] Standard, B. (2005). Eurocode 8: Design of structures for earthquake resistance, Part, 1, pp. 1991–8.

[21] UBC. (1994). UBC 1994, International conference of Building officials, Whittier, California, vol. 63.

[22] CSI (Computers and Structures, I.. (2010). CSI analysis reference manual for SAP2000, ETABS, SAFE and CSiBridge, ,.

[23] ASCE. (2000). American Society of Civil Engineers, Fema 356 Prestandard and Commentary for the Seismic Rehabilitation of Building, Rehabilitation, (November),.

[24] Paulay, T., Priestley, M.J.N. (1992). Seismic design of reinforced concrete and masonry buildings, vol. 768, Wiley New York.

[25] Lian, M., Zhou, Y., Wang, Y., Su, M. (2024). Experimental investigation of mechanical properties of NiTi superelastic shape memory alloy cables, J. Constr. Steel Res., 214, pp. 108447.

[26] (N.d.). Modeling of Superelastic Shape Memory Alloy Elements - Technical Knowledge Base - Computers and Structures, Inc. - Technical Knowledge Base. Available at: https://wiki.csiamerica.com/display/kb/Modeling+of+Superelastic+Shape+Memory+Alloy+Elements. [accessed January 22, 2024].

[27] (N.d.). PEER Ground Motion Database - PEER Center. Available at: https://ngawest2.berkeley.edu/spectras/new?sourceDb_flag=1. [accessed April 22, 2024].

[28] (N.d.). SeismoMatch - Response Spectrum Matching - Seismosoft. Available at: https://seismosoft.com/products/seismomatch/. [accessed April 22, 2024].

[29] TahamouliRoudsari, M., Entezari, A., Hadidi, M.H., Gandomian, O. (2017). Experimental Assessment of Retrofitted RC Frames With Different Steel Braces, Structures, 11(January), pp. 206–17, Doi: 10.1016/j.istruc.2017.06.003.